AD-A175 671 ANALYZED POTENTIAL VORTICITY FIELDS FOR EXPLOSIVE AND NON-EXPLOSIVE CYCLO (U) NAVAL POSTGRADUATE SCHOOL MONTEREY CA P J KIRCHOFFER SEP 86 1/1

UNCLASSIFIED F/G 4/1 NL

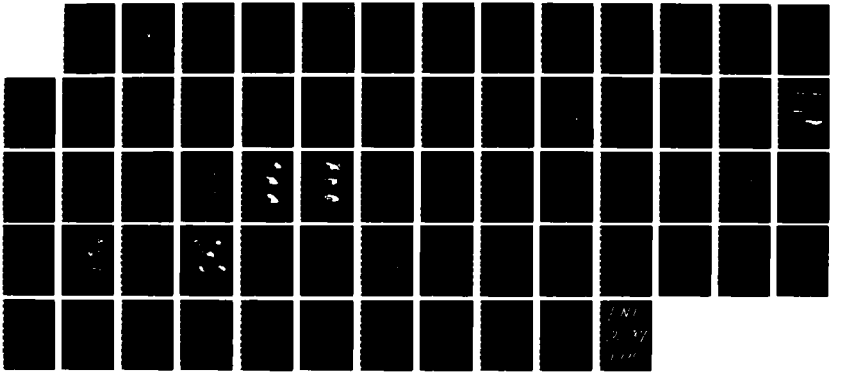

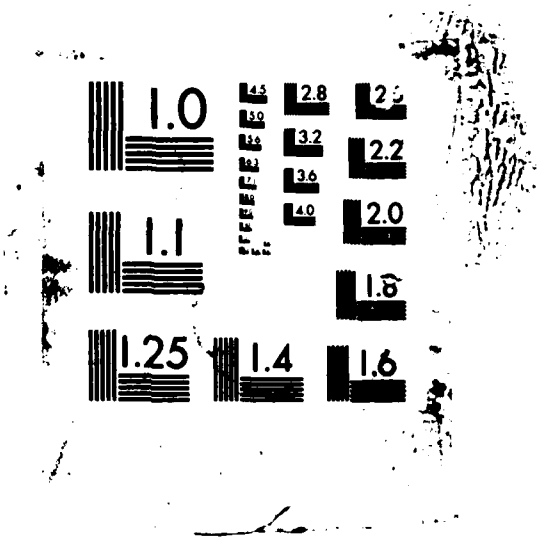
1.0
1.1
1.25
1.4
1.6
2.8
3.2
3.6
4.0
2.2
2.0
1.8

NAVAL POSTGRADUATE SCHOOL
Monterey, California

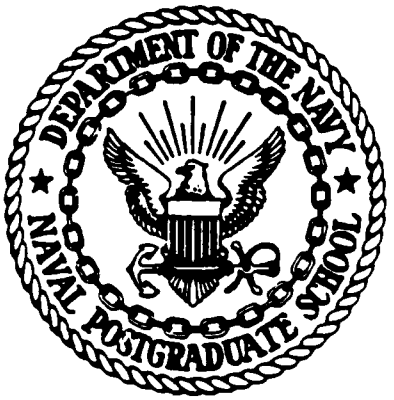

THESIS

ANALYZED POTENTIAL VORTICITY FIELDS
FOR EXPLOSIVE AND NON-EXPLOSIVE
CYCLOGENESIS EVENTS DURING FGGE

by

Peter J. Kirchoffer

September 1986

Thesis Advisor: R. L. Elsberry

Approved for public release; distribution is unlimited.

SECURITY CLASSIFICATION OF THIS PAGE

AD-A175 671

REPORT DOCUMENTATION PAGE

1a REPORT SECURITY CLASSIFICATION: Unclassified	1b. RESTRICTIVE MARKINGS
2a SECURITY CLASSIFICATION AUTHORITY	3 DISTRIBUTION/AVAILABILITY OF REPORT: Approved for public release; distribution is unlimited
2b DECLASSIFICATION/DOWNGRADING SCHEDULE	
4 PERFORMING ORGANIZATION REPORT NUMBER(S)	5. MONITORING ORGANIZATION REPORT NUMBER(S)
6a. NAME OF PERFORMING ORGANIZATION: Naval Postgraduate School / 6b OFFICE SYMBOL (If applicable): Code 63	7a. NAME OF MONITORING ORGANIZATION: Naval Postgraduate School
6c ADDRESS (City, State, and ZIP Code): Monterey, California 93943-5000	7b. ADDRESS (City, State, and ZIP Code): Monterey, California 93943-5000
8a NAME OF FUNDING/SPONSORING ORGANIZATION / 8b. OFFICE SYMBOL (If applicable)	9. PROCUREMENT INSTRUMENT IDENTIFICATION NUMBER
8c ADDRESS (City, State, and ZIP Code)	10 SOURCE OF FUNDING NUMBERS: PROGRAM ELEMENT NO / PROJECT NO / TASK NO / WORK UNIT ACCESSION NO

11 TITLE (Include Security Classification)

ANALYZED POTENTIAL VORTICITY FIELDS FOR EXPLOSIVE AND NON-EXPLOSIVE CYCLOGENESIS EVENTS DURING FGGE

12 PERSONAL AUTHOR(S): Kirchoffer, Peter J.

13a TYPE OF REPORT	13b TIME COVERED	14 DATE OF REPORT (Year, Month, Day)	15 PAGE COUNT
Master's Thesis	FROM _____ TO _____	1986 September	64

16 SUPPLEMENTARY NOTATION

17 COSATI CODES			18 SUBJECT TERMS (Continue on reverse if necessary and identify by block number)
FIELD	GROUP	SUB-GROUP	Potential vorticity, jet streaks, explosive cyclogenesis, vorticity advection

19 ABSTRACT (Continue on reverse if necessary and identify by block number)

Potential vorticity and jet streak properties associated with 23 explosive and non-explosive cyclones from the western North Atlantic and western North Pacific Oceans are analyzed for ~~the period~~ 17 January ~~to~~ 23 February 1979. ECMWF analyses with FGGE data are used to represent the 300 mb winds over these ocean areas. Relative maxima in potential vorticity are present upstream of all cyclones. Storm tracks with respect to the potential vorticity maxima are counter-clockwise with the greatest sea-level pressure decreases occurring when the storm is to the east or southeast of the maximum, whereas pressure falls diminish when the cyclone is north of the maximum. Only five of the 23 cases have a pre-existing potential vorticity lobe that becomes superposed with the surface feature and enhances cyclogenesis. In the remaining cases, the cyclone and potential vorticity lobe propagate and develop concurrently. The presence of a jet maxima over the storm is a major factor in storm development with large pressure falls being directly related to higher 300 mb wind speeds. In 20 of 23 cases, the storm is in —

20 DISTRIBUTION/AVAILABILITY OF ABSTRACT	21 ABSTRACT SECURITY CLASSIFICATION
☒ UNCLASSIFIED/UNLIMITED ☐ SAME AS RPT ☐ DTIC USERS	Unclassified
22a NAME OF RESPONSIBLE INDIVIDUAL: Russell L. Elsberry	22b TELEPHONE (Include Area Code): 408- 646-2373 / 22c OFFICE SYMBOL: 63 Es

DD FORM 1473, 84 MAR — 83 APR edition may be used until exhausted. All other editions are obsolete.

SECURITY CLASSIFICATION OF THIS PAGE

the left front jet quadrant at some time during its development. A statistical analysis demonstrates that forecasting the actual values of 12-h pressure falls from the potential vorticity and wind fields is difficult. However, forecasting development within one of three intensity categories using a discriminate analysis technique may approach 90% accuracy for explosive cyclones. (Tl e sos)

Approved for public release; distribution is unlimited.

Analyzed Potential Vorticity Fields
for Explosive and Non-explosive
Cyclogenesis Events During FGGE

by

Peter J. Kirchoffer
Lieutenant, United States Navy
B.S., University of Wisconsin-Madison, 1979

Submitted in partial fulfillment of the
requirements for the degree of

MASTER OF SCIENCE IN METEOROLOGY AND OCEANOGRAPHY

from the

NAVAL POSTGRADUATE SCHOOL
September 1986

Author: Peter J. Kirchoffer
Peter J. Kirchoffer

Approved by: R. L. Elsberry
R. L. Elsberry, Thesis Advisor

C. H. Wash
C. H. Wash, Second Reader

R. J. Renard
R. J. Renard, Chairman,
Department of Meteorology

J. N. Dyer
J. N. Dyer,
Dean of Science and Engineering

ABSTRACT

Potential vorticity and jet streak properties associated with 23 explosive and non-explosive cyclones from the western North Atlantic and western North Pacific Oceans are analyzed for the period 17 January to 23 February 1979. ECMWF analyses with FGGE data are used to represent the 300 mb wind fields over these ocean areas. Relative maxima in potential vorticity are present upstream of all cyclones. Storm tracks with respect to the potential vorticity maxima are counter-clockwise with the greatest sea-level pressure decreases occurring when the storm is to the east or southeast of the maximum, whereas pressure falls diminish when the cyclone is north of the maximum. Only five of the 23 cases have a pre-existing potential vorticity lobe that becomes superposed with the surface feature and enhances cyclogenesis. In the remaining cases, the cyclone and potential vorticity lobe propagate and develop concurrently. The presence of a jet maxima over the storm is a major factor in storm development with large pressure falls being directly related to higher 300 mb wind speeds. In 20 of 23 cases, the storm is in the left-front jet quadrant at some time during its development. A statistical analysis demonstrates that forecasting the actual values of 12-h pressure falls from the potential vorticity and wind fields is difficult. However, forecasting development within one of three intensity categories using a discriminate analysis technique may approach 90% accuracy for explosive cyclones.

TABLE OF CONTENTS

I. INTRODUCTION 8

II. REVIEW OF RECENT STUDIES 13

III. DATA DESCRIPTION 19

A. POTENTIAL VORTICITY CALCULATIONS 19

B. COMPARISON OF VERTICAL CROSS-SECTIONS 19

C. HORIZONTAL MAPS OF POTENTIAL VORTICITY 26

IV. RESULTS 33

A. BACKGROUND 33

B. CASE STUDIES 34

C. POTENTIAL VORTICITY AND JET STREAK QUALITATIVE RESULTS 45

V. STATISTICAL RESULTS 50

VI. CONCLUSIONS 58

LIST OF REFERENCES 60

INITIAL DISTRIBUTION LIST 62

LIST OF FIGURES

1.1 Storm tracks and positions of explosive (solid) and non-explosive (dashed) cyclones in the North Pacific Ocean (Smith, 1986) 9

1.2 As in Fig. 1.1 except for North Atlantic Storms (Smith, 1986) 10

2.1 Schematic of mean circulation relative to the tropopause, including a folded tropopause (Danielson, 1968) 14

2.2 Potential vorticity and ozone within a tropopause fold based on aircraft observations normal to a jet streak 16

2.3 Schematics of cyclogenesis associated with the arrival of an upper-air IPV anomaly over a low level baroclinic region 18

3.1 Cross-sections normal to a jet streak for the Presidents Day storm (Uccellini et al. 1985) 21

3.2 Isentropes (3°K interval) from ECMWF analyses for similar cross-section as in Fig. 3.1 21

3.3 Potential vorticity ($x10^6$ °K/s/mb) from ECMWF analyses for similar cross-section as in Fig. 3.1. Contour interval 2.5, (3.0) for top (bottom) 22

3.4 Isotachs (5 m/s interval) from ECMWF analyses for similar cross-section as in Fig. 3.1 23

3.5 Relative humidity (3% interval) from ECMWF analyses for similar cross-section as in Fig. 3.1 24

3.6 Potential vorticity ($x10^6$ °K/s/mb) analyzed on 292°K surface. See description in text (Uccellini et al. 1985) 28

3.7 Sectors of the 300°K IPV maps for the period 20-25 Sept 1982. See description in text (Hoskins, 1985) 29

3.8 Potential vorticity and relative humidity at 300, 400 and 500 mb at 12 GMT 18 Feb for the Presidents Day storm 29

3.9 As in Fig. 3.8, except for 300 mb at 18 GMT 18 Feb (top), 00 GMT 19 Feb (middle) and 06 GMT 19 Feb 1979 (bottom) 30

4.1 Potential vorticity and winds at 300 mb for the Presidents Day storm. Reference position is 37.5°N /67.5°W 36

4.2 As in Fig. 4.1, except for Pacific cyclone (P-2). Reference position is 37.5°N /150.0°E 38

4.3 As in Fig. 4.1, except for Pacific cyclone (P-3). Reference position is 37.5°N /142.5°E 40

4.4 As in Fig. 4.1, except for Atlantic cyclone (A-4). Reference position is 37.5°N /67.5°W 41

4.5 As in Fig. 4.4, except dotted lines represent positive vorticity advection (PVA) 43

4.6 As in Fig. 4.1, except for Atlantic cyclone (NA-2). Reference position is 45.0°N /67.5°W 44

4.7 Schematic evolution of a potential vorticity lobe and a surface cyclone for the case in which the lobe and the cyclone become superposed 46

4.8 As in Fig. 4.7, except for the case in which the potential vorticity lobe and cyclone develop concurrently 46

5.1 Expected development (Low, Moderate, Explosive) of Atlantic (ATL) and Pacific (PAC) storms from discriminate analysis 57

I. INTRODUCTION

Rapidly deepening maritime cyclones have received much attention due to their potential danger to maritime operations and the failure of operational numerical weather prediction models to provide a warning for these developments. Numerous investigators have studied jet streaks and their associated divergence patterns to find relationships between jet streaks and cyclogenesis (e.g., Hovanec and Horn, 1975; Newton, 1956; Reiter, 1969). In a climatological study of explosively developing cyclones, Sanders and Gyakum (1980) found that they were most likely to occur within or poleward of the main belt of westerlies. In a study of the Presidents' Day storm of 1979, Uccellini et al. (1984) found that an intensifying subtropical jet and a polar front jet within a deepening trough were major contributors to explosive cyclogenesis off the east coast of the U.S. In a subsequent study of the Presidents' Day storm, Uccellini et al. (1985) suggested that superposition of high values of potential vorticity that had earlier been forced downward by transverse vertical circulations within the jet may have contributed to explosive deepening of that storm. However, Gyakum (1983) observed a large increase in potential vorticity that was concurrent with the intensification of the Queen Elizabeth II (QE II) storm. Hoskins et al. (1985) tracked a high potential vorticity region that broke off from the main "reservoir" and became stagnant near a developing cut-off cyclone in the North Atlantic Ocean.

The emphasis of this research is to determine whether superposition or concurrent development of high values of potential vorticity above a surface disturbance are most frequently associated with explosive deepening of the storm. This study examines 23 cyclones in the western North Pacific and western North Atlantic Oceans (Figs. 1.1 and 1.2), which are the most favorable regions for maritime explosive cyclogenesis (Sanders and Gyakum, 1980). The cyclones (Smith, 1986) are of varying intensity and are studied for a minimum of 30 hours during their development (Table 1). Storm development is also correlated with positive vorticity advection (PVA), 300 mb wind speed above the storm, position relative to the jet, and the initial latitude.

Studies of maritime cyclogenesis have been hampered by the lack of reporting stations over the ocean. The First GARP (Global Atmospheric Research Program) Global Experiment (FGGE) was a vigorous effort to enhance global data coverage,

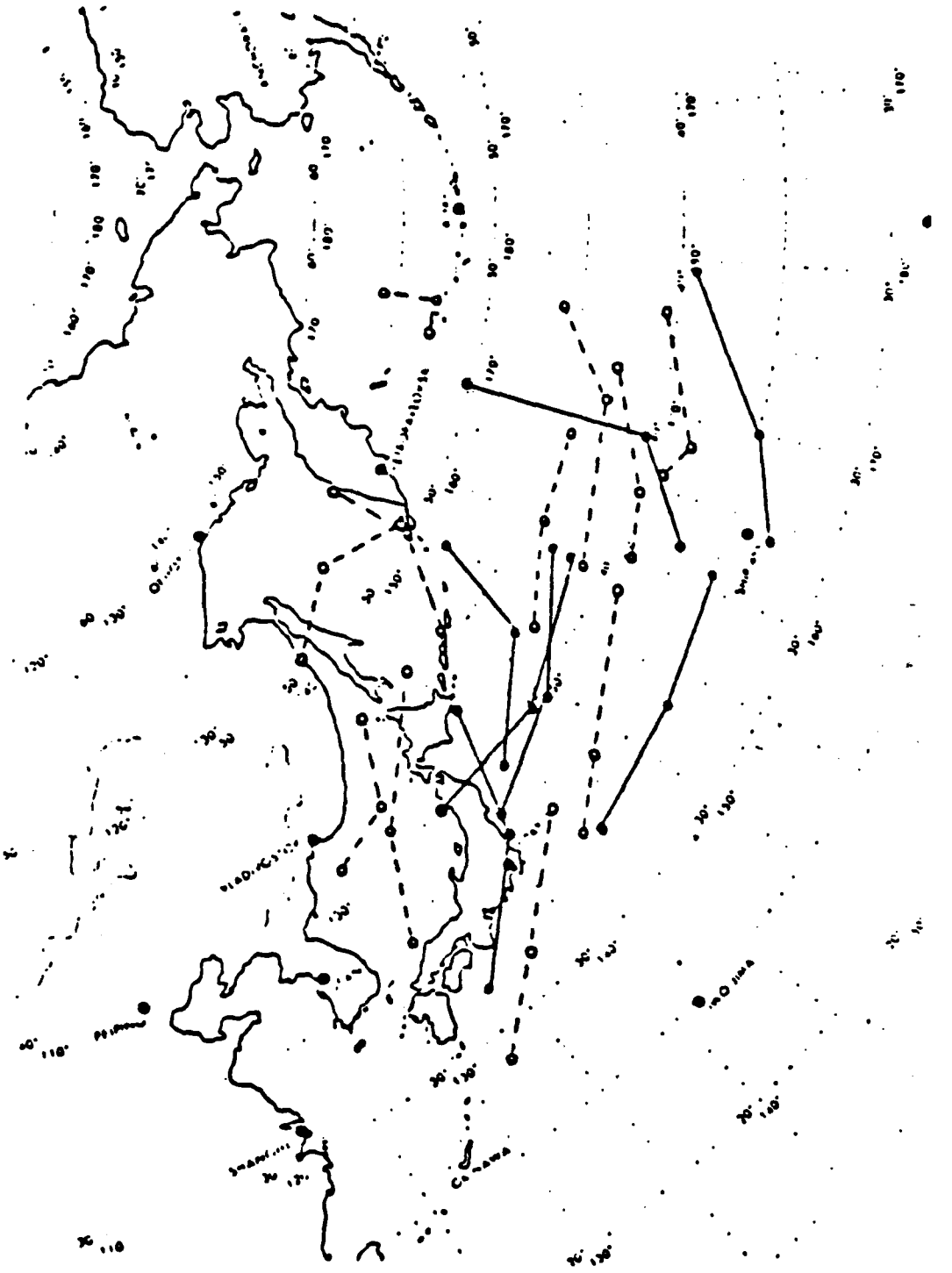

Fig. 1.1 Storm tracks and positions of explosive (solid) and non-explosive (dashed) cyclones in the North Pacific Ocean (Smith, 1986).

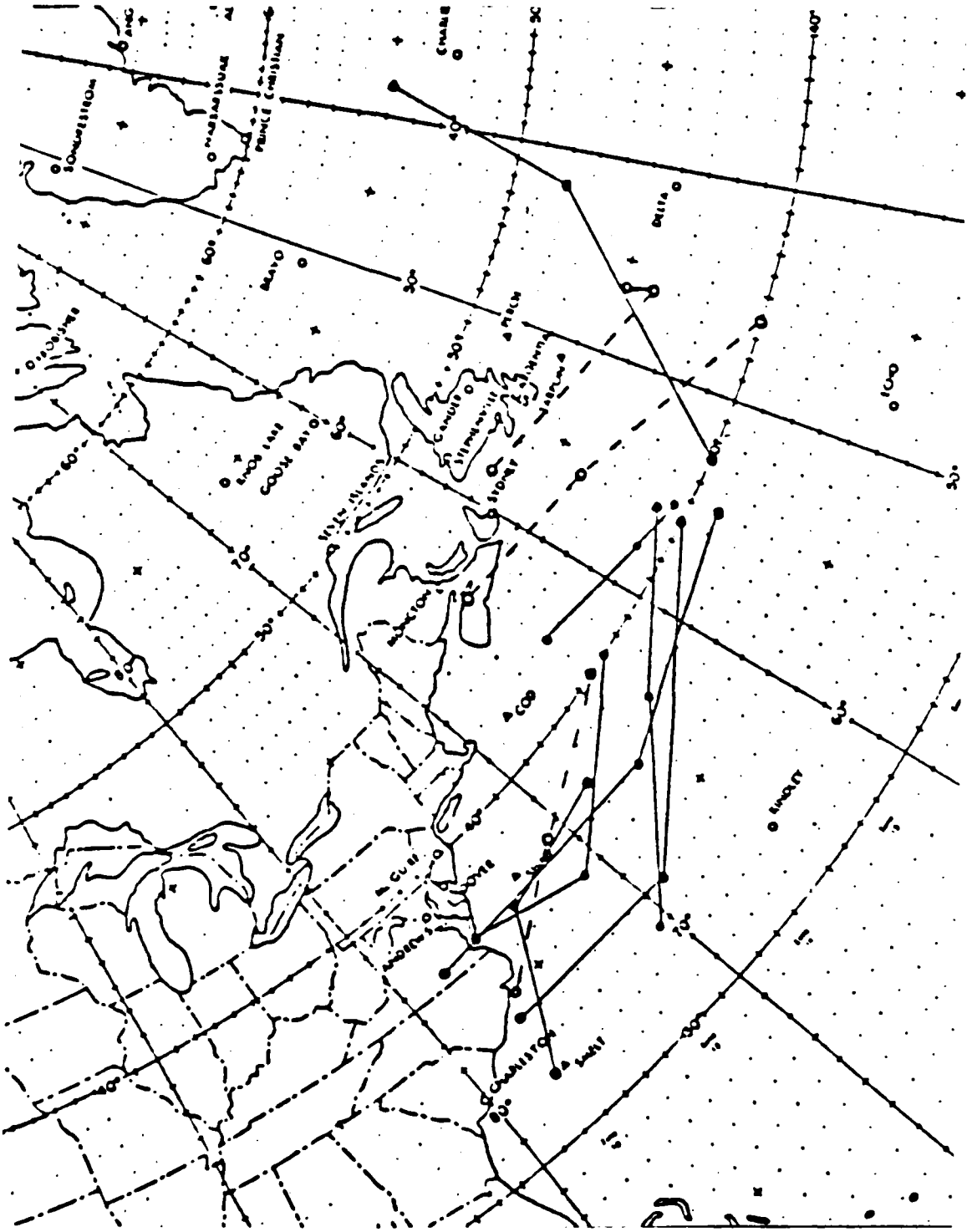

Fig. 1.2 As in Fig. 1.1 except for North Atlantic Storms (Smith, 1986).

TABLE 1. LIST OF CYCLONES

List of cyclones and 24-h sea level pressure changes (mb) not corrected for latitude. P and A denote explosive cyclones for the North Pacific Ocean and North Atlantic Ocean respectively. NP and NA denote non-explosive cyclones for the North Pacific Ocean and North Atlantic Ocean respectively. (Smith, 1986).

PACIFIC

Explosive Cases

Lows	NMC	ECMWF	Date
P1	33	35	18 Jan 1979
P2	18	22	26 Jan 1979
P3	24	23	05 Feb 1979
P4	20	20	09 Feb 1979
P5	23	21	17 Feb 1979
P6	24	19	15 Feb 1979
P7	22	20	24 Jan 1979

Non-explosive

NP1	7	3	21 Jan 1979
NP2	13	15	31 Jan 1979
NP3	0	2	04 Feb 1979
NP4	5	2	04 Feb 1979
NP5	5	4	08 Feb 1979
NP6	16	11	13 Feb 1979
NP7	12	12	14 Feb 1979
NP8	18	11	21 Feb 1979
NP9	12	7	19 Feb 1979
NP10	21	16	13 Feb 1979
NP11	22	7	28 Jan 1979

ATLANTIC

Explosive Cases

A1	25	30	18 Jan 1979
A2	30	24	28 Jan 1979
A3	30	35	01 Feb 1979
A4	23	21	09 Feb 1979
A5	26	23	13 Feb 1979
A6	22	27	19 Feb 1979
A7	14	20	15 Feb 1979

Non-explosive

NA1	12	13	07 Feb 1979
NA2	5	11	22 Feb 1979
NA3	22	7	23 Jan 1979

especially in data sparse regions. FGGE data was compiled from numerous sources to provide a complete set of global analyses twice daily with a horizontal resolution of at least 500 km. Analyses from the European Centre for Medium-Range Weather Forecasts (ECMWF) during FGGE provide the most complete data set available (Halem et al. 1982).

Even though the operational numerical models do not predict explosive cyclogenesis events, the precursor conditions might be represented in the initial analyses and forecasts. Using the ECMWF analyses as "perfect progs", the upper-level wind and associated potential vorticity fields are examined in relation to explosively and non-explosively developing cyclones. The goal is to determine the feasibility of using similar operationally analyzed and predicted fields to improve warnings of explosively developing cyclones.

Chapter II will summarize previous research on upper-level fronts and potential vorticity in relation to cyclogenesis. Chapter III outlines the procedure to calculate potential vorticity and presents a test case in which vertical cross-sections obtained from the ECMWF analyses are compared to cross sections obtained from radiosonde data. Maps of potential vorticity , relative humidity, and vertical motion on the 500, 400 and 300 mb pressure surfaces are studied to determine their usefulness as a potential forecast aid. Results of case studies of potential vorticity, PVA, and jet streak contributions to explosive cyclogenesis are presented in Chapter IV. A statistical summary comparing and contrasting the results found in the Atlantic and Pacific Oceans is presented in Chapter V. Chapter VI discusses the conclusions and provides suggestions for follow-on research.

II. REVIEW OF RECENT STUDIES

The superposition of high values of potential vorticity found within upper-level fronts has been cited as a possible triggering mechanism for the formation of extratropical cyclones (Uccellini et al. 1985). Shapiro (1980) defines potential vorticity on isentropic (potential temperature) surfaces as the absolute vorticity of an air parcel times the thermal stability. Although upper-level fronts and their associated tropopause folds have been known to exist since the early 1950's, the effects of upper-level frontogenesis on explosively developing cyclones have been documented in only a few cases due to the large amount of data required to resolve the vertical structure. Since this study examines cyclogenesis in data sparse regions over the oceans, data analysis and interpretation are difficult and subject to error.

Tropopause "folding" as defined by Reed (1955) is considered to be a mechanism for detaching stratospheric air from the main "reservoir" and transporting this air toward the mid-troposphere along the axis of the jet stream. Danielson (1968) confirmed the hypothesis proposed by Reed that tropopause folding is one mechanism for upper-level frontogenesis, and that large values of potential vorticity frequently observed in upper-level fronts have a stratospheric source. Tropopause folds tend to occur to the west of developing troughs along the axis of confluence between direct and indirect circulation cells beneath the core of the jet (Fig. 2.1). Upper-level fronts that are located in the negative vorticity region between the trough and the upstream ridge are found to be in a region of sinking motion with the strongest subsidence near the warm edge of the front. This sinking of the warmer air (indirect circulation) intensifies the temperature gradient due to adiabatic warming. Shapiro (1970) concluded from his study of a mid-latitude cyclone that intense baroclinic processes within and on the scale of upper-level frontal zones are an essential ingredient in extratropical cyclogenesis.

In a numerical study, Bleck (1974) showed how a potential vorticity field evolved in time and influenced cyclonic development at the surface. He found a correlation between the downward extrusion of high potential vorticity and development of the surface cyclone. During the first 24 hours of storm development, a potential vorticity extrusion reached down below the 500 mb level and enhanced the stretching mechanism by which cyclonic vorticity is generated.

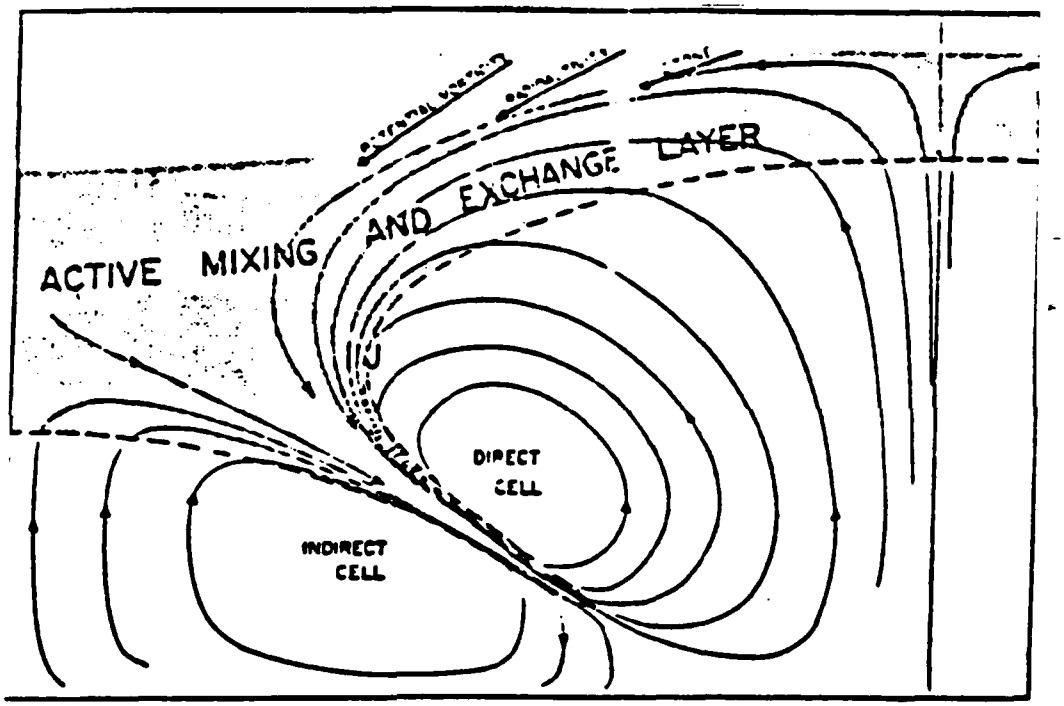

Fig. 2.1 Schematic of mean circulation relative to the tropopause, including a folded tropopause (Danielson, 1968).

Shapiro (1978) used an aircraft-mounted ozone detector to determine the distribution of atmospheric ozone concentrations in the vicinity of an upper-level jet stream-frontal system. He showed the characteristic downward extrusion of stratospheric air into the troposphere contained a high concentration of ozone (Fig. 2.2). Although the potential vorticity of an air parcel would be conserved in adiabatic and frictionless flow, Shapiro showed that turbulent mixing processes cannot be neglected. Uccellini et al. (1985) proposed that as stratospheric air descends into the troposphere, vortex tubes are stretched and static stability decreases significantly. If the stratospheric values of potential vorticity are to be conserved, the absolute vorticity (measured on isentropic surfaces) should increase in the troposphere. In one case in which potential vorticity was not conserved, Gyakum (1983) found that a large increase in potential vorticity in the QE II storm was probably due to bulk heating effects associated with cumulus convection. The most likely bulk heating effect responsible for the warm-core explosive cyclogenesis and potential vorticity generation appeared to be cumulus-induced compensating subsidence.

In a recent study of the Presidents' Day cyclone of 18-19 February 1979, Uccellini et al. (1985) observed tropopause folding far to the west associated with rapid amplification of a polar jet-trough system 12-24 h prior to rapid cyclogenesis off the east coast of the U.S. Twelve hours prior to the occurrence of rapid cyclogenesis, stratospheric air was near the 800 mb level and was moving rapidly to a position just to the west of the developing cyclone. Based on an extrapolated position over the ocean, the stratospheric extrusion and associated high potential vorticity were thought to be nearly above the storm center as explosive deepening of the surface vortex occurred. Uccellini et al. (1985) state that the explosive development of the cyclone was enhanced by the descent of stratospheric air and the extension of high potential vorticity to lower levels. This study emphasized the folded tropopause as a pre-existing entity whose formation and propagation was completely separated from the surface disturbance. In another study of the Presidents' Day Storm, Bosart and Lin (1984) also found that the rapid cyclogenesis stage was marked by the approach of a potential vorticity maximum in the mid and upper troposphere.

Hoskins et al. (1985) tracked a high potential vorticity region as it became elongated and eventually broke off from the main "reservoir" to the north before being advected into an area just prior to where rapid cyclogenesis would occur. Hoskins showed how an upper-level cyclonic rotation induces warm air advection to the east of

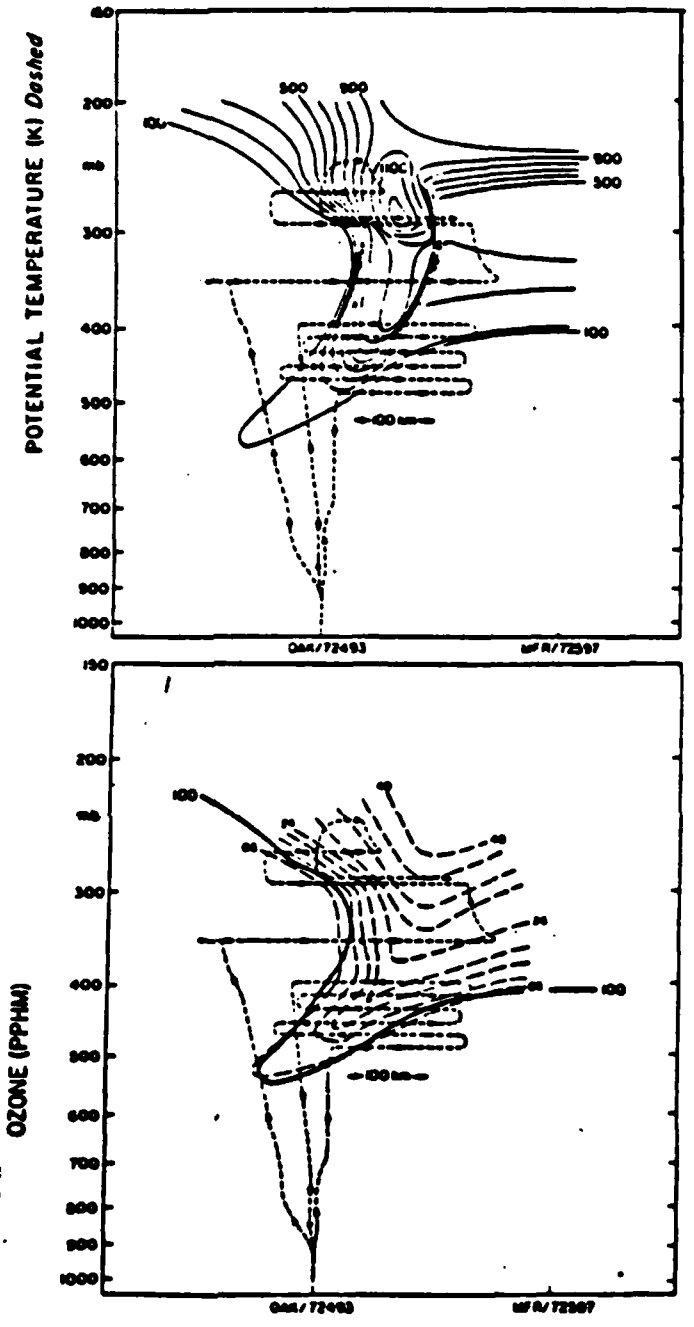

Fig. 2.2 (top) Potential vorticity ($x10^6$ °K/s/mb) and (bottom) ozone (pphm/vol) (dashed) with superposed 100 unit potential vorticity isoline (solid) based on aircraft observations normal to jet stream (Shapiro, 1978).

the vorticity maximum and contributes to cyclone development at the surface (Fig. 2.3). This occurs when a cyclonic, upper-air isentropic potential vorticity (IPV) anomaly arrives above a low-level baroclinic region and induces a cyclonic rotation near the surface that contributes to a warm temperature anomaly somewhat ahead of the upper-level IPV anomaly. Since the upper-level equatorward flow is advecting stratospheric air of relatively high potential vorticity compared to the poleward tropospheric air with lower potential vorticity, the upper-level circulation induced by the surface potential temperature anomaly will tend to reinforce the upper-air IPV anomaly.

Although high potential vorticity of stratospheric origin has been found in the lower troposphere, it is not certain what effect this has on explosively developing cyclones. This thesis will attempt to determine the effects of potential vorticity on maritime cyclogenesis by studying explosive and non-explosive cases. In the following chapter, an attempt will be made to determine how much resolution of the potential vorticity field is lost by comparing vertical cross-sections from Uccellini et al. (1985) to cross-sections derived from the mandatory levels only.

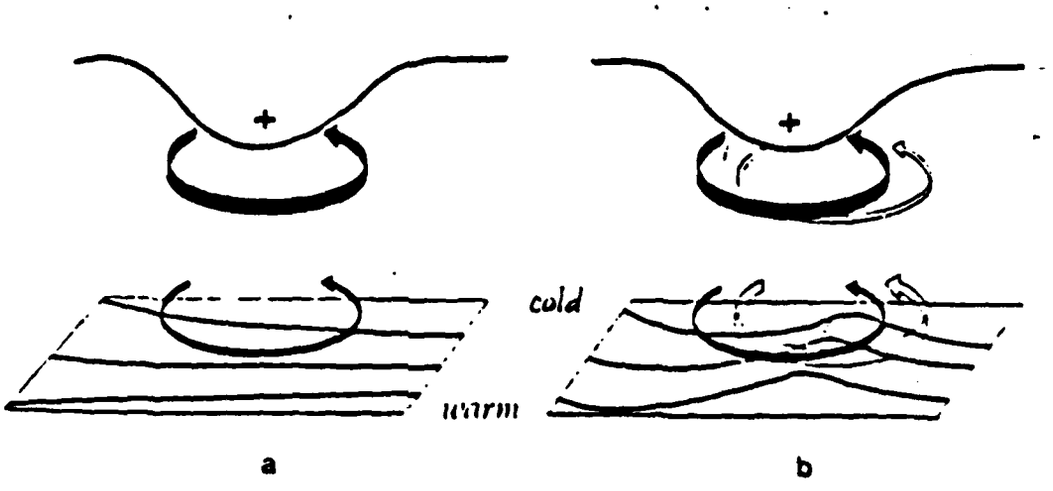

Fig. 2.3 Schematics of cyclogenesis associated with the arrival of an upper-air IPV anomaly (plus sign) over a low-level baroclinic region. See description in text. (Hoskins et al. 1985).

III. DATA DESCRIPTION

A. POTENTIAL VORTICITY CALCULATIONS

Potential vorticity was computed on a three-dimensional array of grid points using the expression from Reed (1955),

$$IPV = (\zeta_p + f)\partial\theta/\partial p - \partial v/\partial p \times \partial\theta/\partial x + \partial u/\partial p \times \partial\theta/\partial y , \qquad (3.1)$$

where IPV is the potential vorticity calculated on a constant pressure surface and converted to an isentropic surface, ζ_p is the relative vorticity on a constant pressure surface, f is the coriolis parameter, θ is the potential temperature, p is the pressure, and u and v are the zonal and meridional components of the wind. The last two terms represent a coordinate transformation from pressure to isentropic coordinates. Potential vorticity values were graphed in vertical cross-sections and on the 300, 400 and 500 mb pressure surfaces after calculation on the ten mandatory pressure levels between 1000 and 100 mb. These potential vorticity fields were calculated from the ECMWF analyses of the FGGE data that consisted of the u and v wind components and the temperature derived from the initialized geopotential analyses via the hydrostatic relation. The grid domain was 45 points in the east/west direction by 25 points in the north/south direction. The grid interval was 1.875 degrees in latitude and longitude. In calculating the terms involving a pressure difference, one-sided differences were taken and assigned to the upper level, because the cross-section plotting program requires values at the mandatory levels.

B. COMPARISON OF VERTICAL CROSS-SECTIONS

Vertical cross-sections from Uccellini et al. (1985) (Figs. 3.1a, 3.1b) were compared to cross-sections derived from the ECMWF gridded data. The purpose of the comparison with Uccellini's cross-sections is to demonstrate how much detail is lost by using the ECMWF analyzed fields only at the mandatory levels. Uccellini's analyses from the Presidents' Day storm of February 1979 over the eastern U.S. were plotted from station rawinsonde data at both the mandatory and significant reporting levels. The FGGE gridded data were plotted by a routine called CROSSX (T.M. Whittaker, University of Wisconsin-Madison), which plots a vertical cross-section

using 6-8 grid points within two degrees latitude of a specified corridor. The parameters displayed by CROSSX include potential temperature (Figs. 3.2a, 3.2b), potential vorticity (Figs. 3.3a, 3.3b), wind component normal to the section (Figs. 3.4a, 3.4b), and relative humidity (Figs. 3.5a, 3.5b).

The isentropic analyses from Uccellini et al. (1985) (Figs. 3.1a, 3.1b) have considerably more detailed structure than the sections from the analyses (Figs. 3.2a, 3.2b). The 296° K to 302° K isentropes in Fig. 3.1a indicate a downward extrusion (tropopause fold) of air with high stability between Huron (HON) and North Platte (LBF). Packing of these isentropes in the mid-troposphere is not evident in the objectively analyzed cross-section (Fig. 3.2a), or in a hand analysis (not shown). More pronounced features such as the areas of high stability between the surface and 750 mb and in the lower stratosphere are relatively similar in the two plots. On the second day, the Uccellini plot (Fig. 3.1b) has an increased packing of the isentropes as the tropopause fold extends farther downward into the troposphere. The section based on the ECMWF analysis (Fig. 3.2b) also has an overall increase in the packing of the isentropes, but the tropopause fold structure is missing. From this comparison, it is apparent that the ECMWF analyses lack the detailed resolution that is necessary to trace the downward extrusion of stratospheric air into the troposphere.

The limitations due to the use of only mandatory level analyses in the ECMWF sections are particularly evident in the potential vorticity comparisons. The tropopause fold, as depicted by the 10 unit potential vorticity value, is more clearly defined in Fig. 3.1a than it is by the 7.5 unit line in Fig. 3.3a. At 400 mb, the maximum values within the fold are almost 20 units in Fig. 3.1a, whereas a maximum value of slightly less than 10 units in found in Fig. 3.3a. At 00 GMT 19 Feb. (Fig. 3.1b), the fold has dipped down to almost 700 mb. This extension of the fold to a lower level is illustrated in Fig. 3.3b with a potential vorticity contour of 12 units that extends only to 470 mb.

The increase in potential vorticity over the 12 hour period can be partially attributed to the increase in the jet speeds as depicted by the plots of normal wind (Figs. 3.1a, 3.1b) and (Figs. 3.4a, 3.4b). The maximum wind speed increases from 45 m/s to 70 m/s and the tropopause fold extends downward on the cyclonic side of the jet in an area of relatively strong horizontal wind shear (Figs. 3.1a, 3.1b). Although not as dramatic, the normal wind components based on the ECMWF analyses (Figs. 3.4a, 3.4b) also show a relatively strong horizontal wind shear on the cyclonic side of the jet where a downward extrusion of relatively high potential vorticity occurs. The 1.875

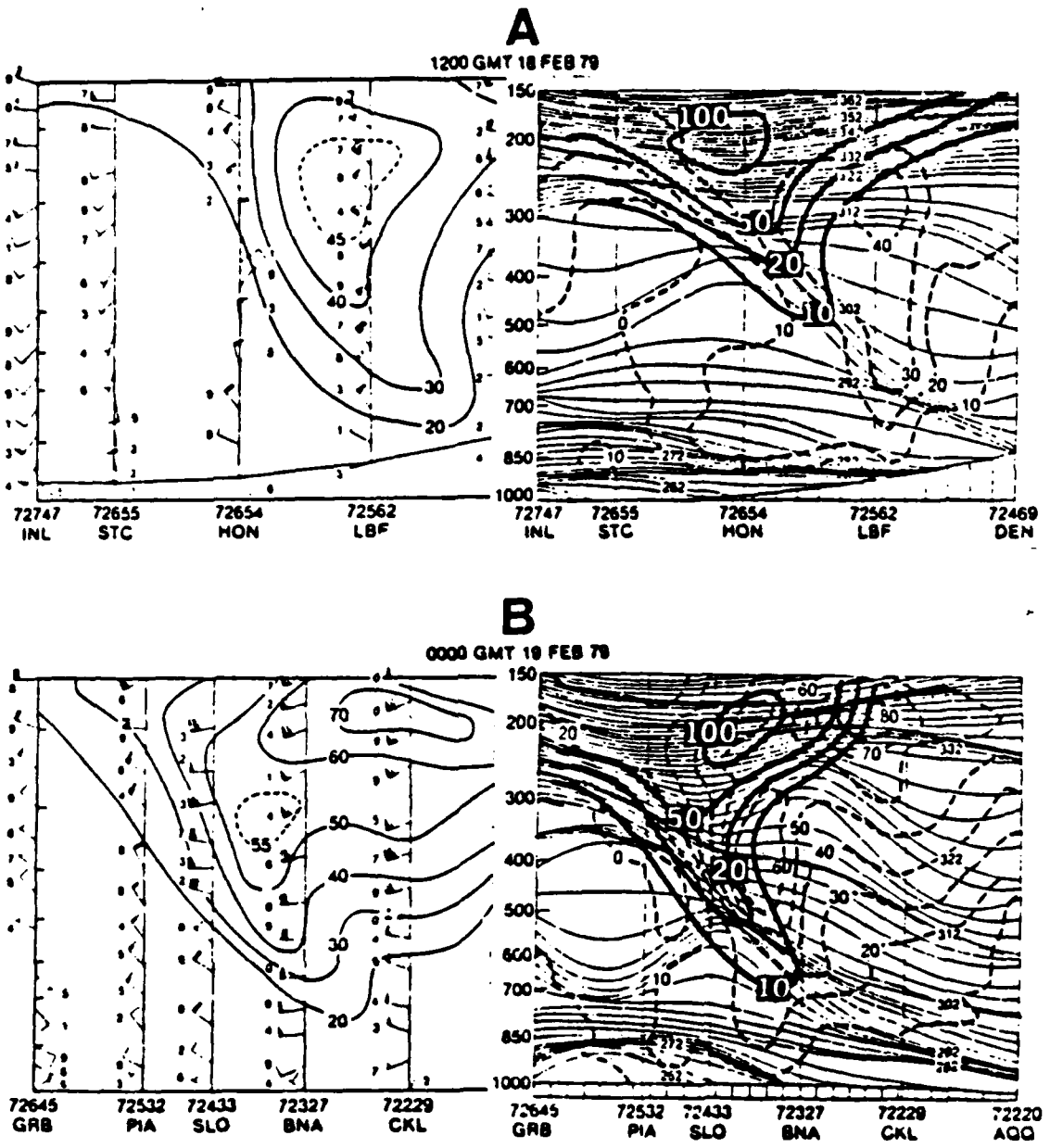

Fig. 3.1 (top) Vertical cross-sections from International Falls, Minnesota (INL) to Denver, Colorado (DEN) for 12 GMT 18 Feb 1979. Isotach analysis (left) depicts total wind speed (m/s). right: Potential vorticity ($x10^6$ °K/s/mb) (dark solid), isentropes °K (light solid) and geostrophic wind (m/s) (dashed). (bottom) As in top except from Green Bay, Wisconsin (GRB) to Apalachicola, Florida (AQQ) for 00 GMT 19 Feb 1979 (Uccellini et al., 1985).

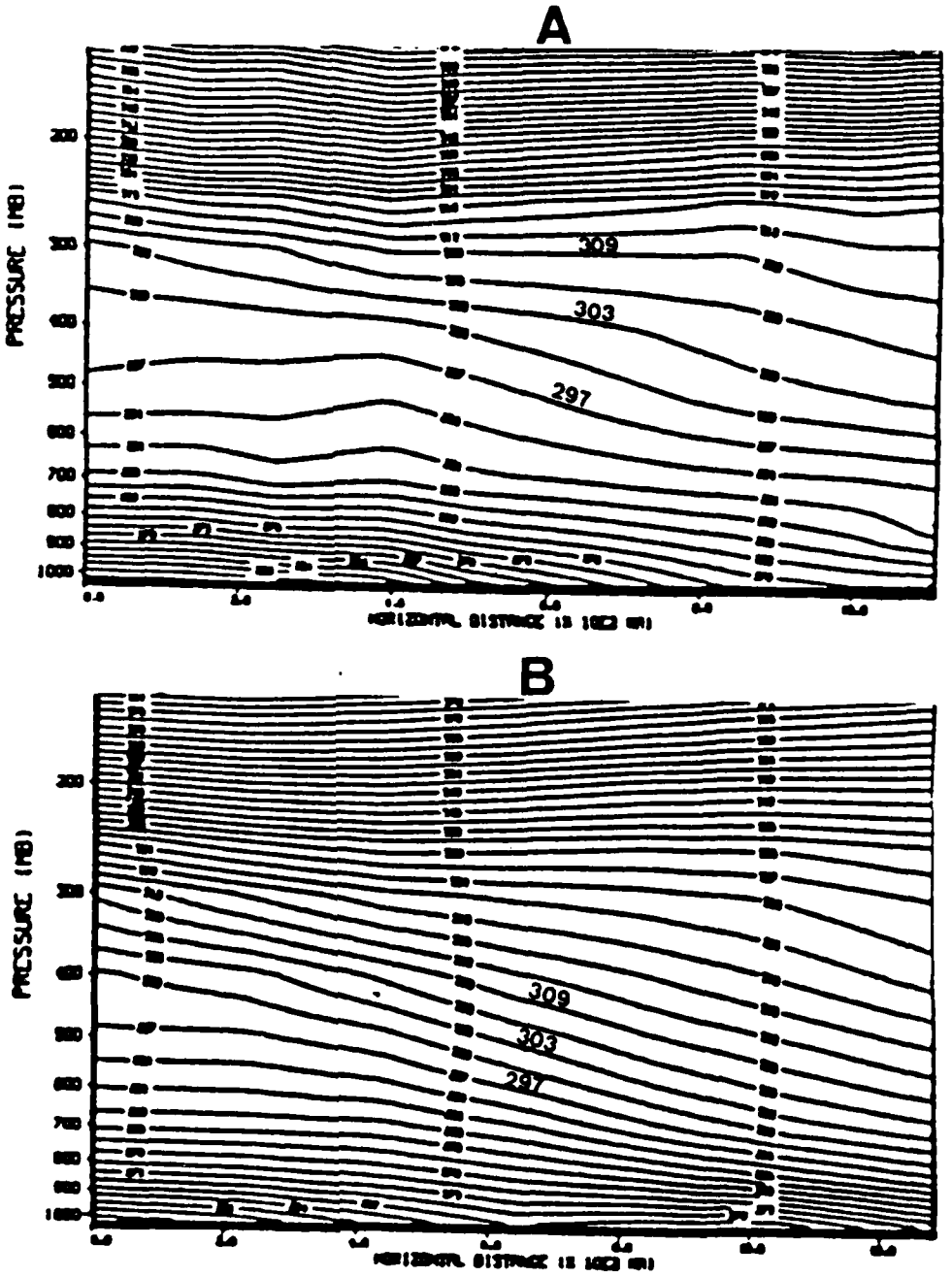

Fig. 3.2 Isentropes (3°K interval) from ECMWF analyses for similar cross-section as in Fig. 3.1.

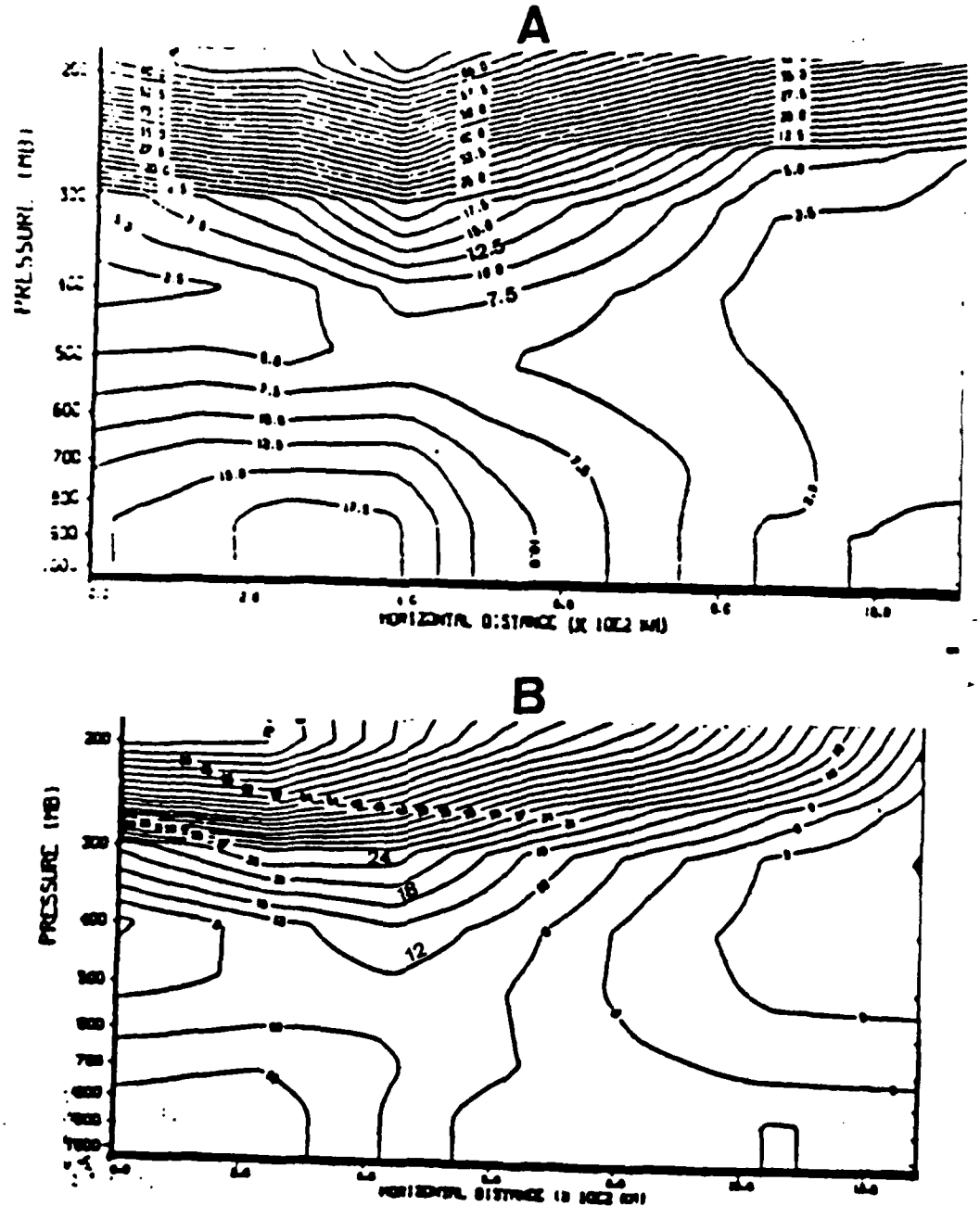

Fig. 3.3 Potential vorticity (x10^6 °K/s/mb) from ECMWF analyses for similar cross-section as in Fig. 3.1. Contour interval 2.5, (3.0) for top (bottom).

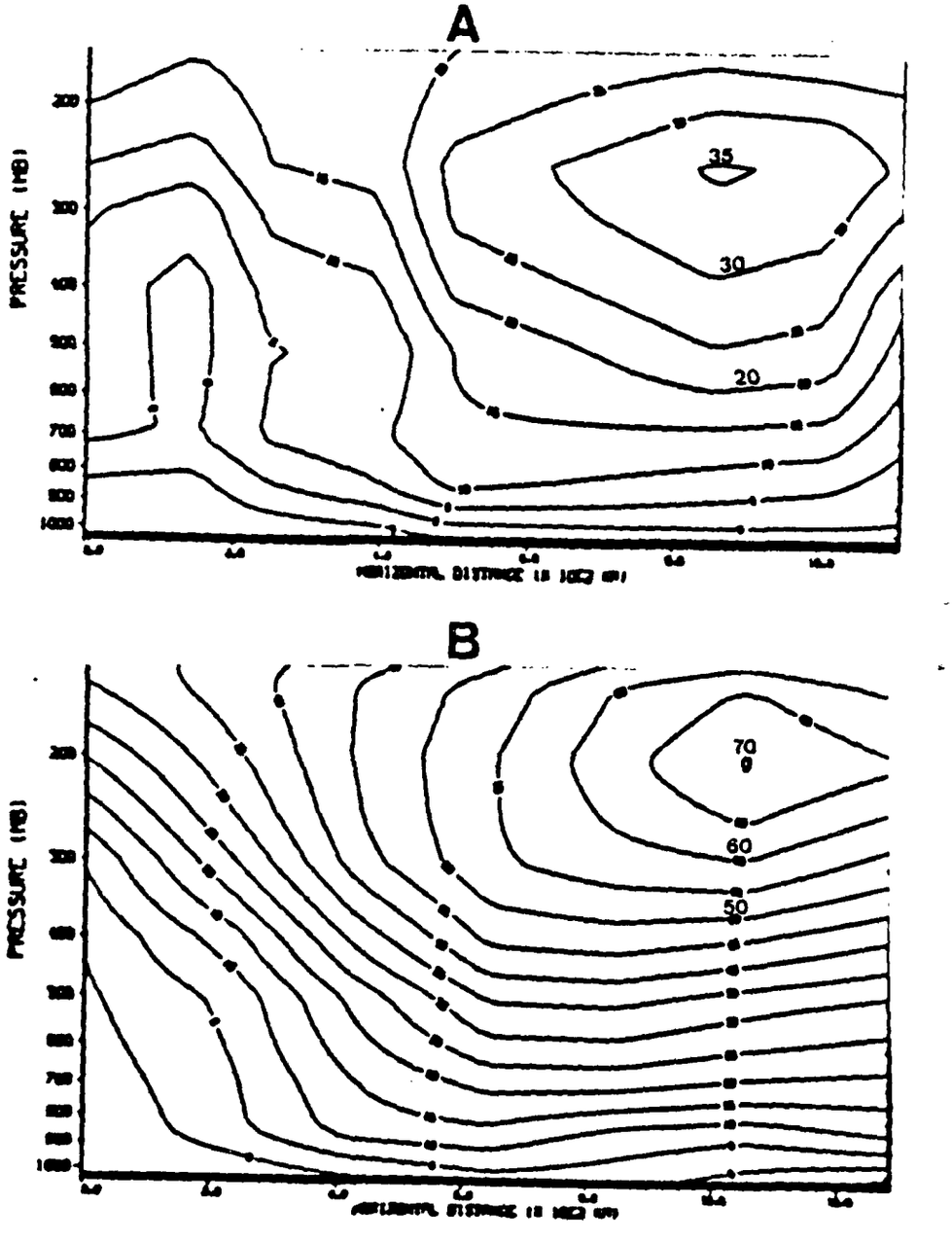

Fig. 3.4 Isotachs (5 m/s interval) from ECMWF analyses for similar cross-section as in Fig. 3.1.

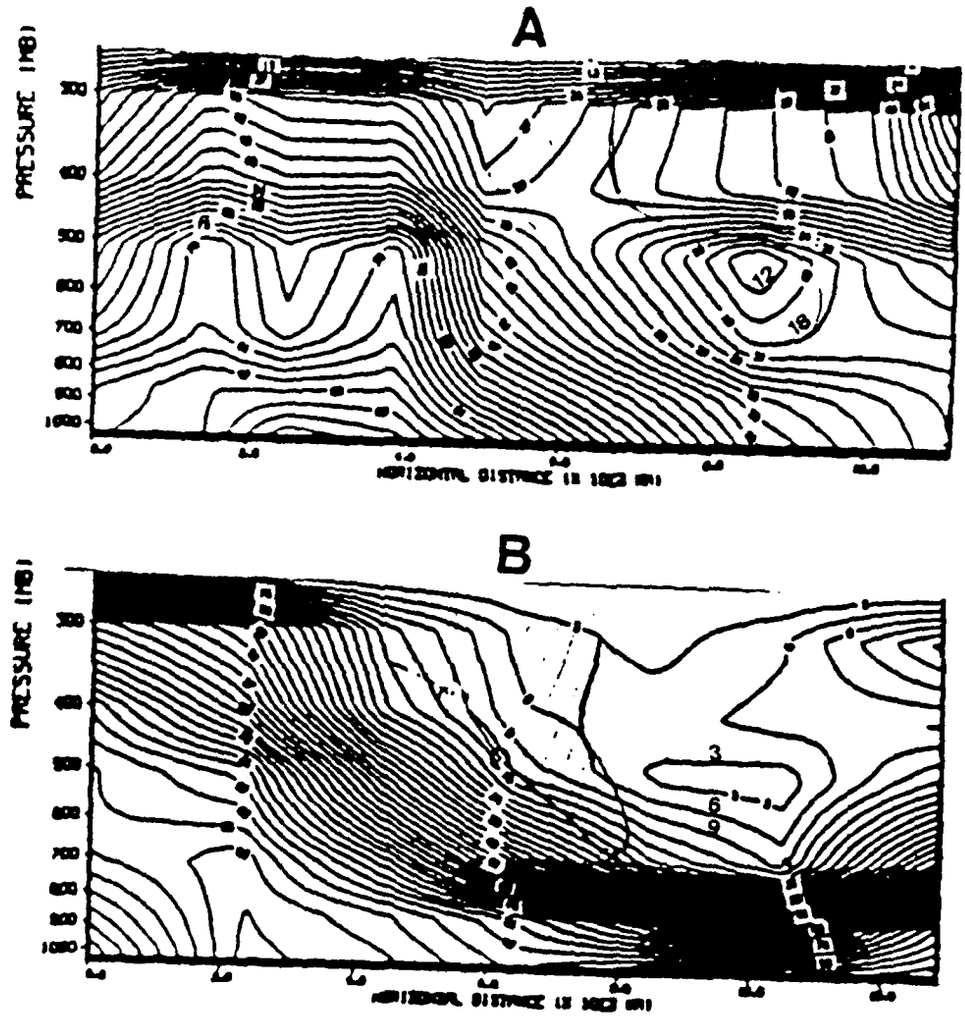

Fig. 3.5 Relative humidity (3% interval) from ECMWF analyses for similar cross-section as in Fig. 3.1.

deg. lat./long. grid is not able to resolve the large wind shears on the cyclonic side of the jet.

Relative humidity was also analyzed since tropopause folds, being of stratospheric origin, may be traced by locating regions of relatively low relative humidity. Because little weight was given to observations, the ECMWF humidity analyses were primarily the first-guess fields from the model. Relative humidity values were not analyzed above 250 mb. The relative humidity section (Fig. 3.5a) has a dry tongue at 300 mb that extends downward and to the right, and has a minimum value of 12 percent at 500 mb. At 00 GMT 19 Feb. (Fig. 3.5b), a very dry area with less than 5 percent relative humidity is found at 500 mb. When Fig. 3.5a is compared to the potential vorticity plot (Fig. 3.3a), the slight downward extrusion of the 7.5 potential vorticity line is associated with a high gradient of relative humidity. The lowest relative humidity values are found to the southwest of the tropopause fold. Comparing Figs. 3.5b and 3.3b, the area of lowest relative humidity is located to the south of the fold as shown by the 12 unit potential vorticity contour. The fold was again in an area of high relative humidity gradient.

In summary, a comparison of Figs. 3.1a and 3.1b with the fields of potential vorticity and potential temperature calculated from ECMWF analyses shows that a great deal of resolution is lost when only mandatory level analyses are available. The potential temperature analyses (Fig. 3.2a, 3.2b) do not have enough vertical and horizontal resolution to define completely the depth of penetration of a tropopause fold. In the Presidents' Day case, the ECMWF potential vorticity analyses do show a slight downward extrusion of relatively high potential vorticity that dipped further downward and increased over a 12-hour period. Large gradients in the relative humidity field and increases in the wind speed and cyclonic shear may also be useful in defining areas where relatively high potential vorticity may occur.

C. HORIZONTAL MAPS OF POTENTIAL VORTICITY

Maps of potential vorticity on the 500, 400 and 300 mb pressure surfaces from the Presidents' Day storm are derived from ECMWF gridded data to determine whether regions with relatively high values of potential vorticity can be identified and tracked to determine their possible impact on explosively developing cyclones. Uccellini et al. (1985) calculated potential vorticity on the 292°K isentropic surface and tracked an area of relatively high potential vorticity in the central U.S. (Fig. 3.6a) to southern

Illinois and Kentucky where the potential vorticity doubled (Fig. 3.6b), and finally to the east coast (Fig. 3.6c) where it is believed to have contributed to rapid cyclogenesis.

In another example, Hoskins et al. (1985) show a sequence of isentropic potential vorticity maps (Fig. 3.7) in which a large area of high potential vorticity air moves rapidly eastward with the strong upper-level winds. By 23 Sept, the high potential vorticity region is greatly elongated and by the 24th it is cut off from the main "reservoir" to the north. On 24 Sept, a cut-off cyclone had formed at 500 mb and a rapidly developing surface cyclone was also present slightly to the east of the high potential vorticity region.

Horizontal plots of potential vorticity (3.1), relative humidity, and vertical motion were obtained each six hours from 12 GMT 18 Feb 79 to 06 GMT 19 Feb 79. At 12 GMT 18 Feb, the 300 mb potential vorticity/ relative humidity map shows a maximum in potential vorticity around 40° N/ 90° W (Fig. 3.8a). Relative humidity values of less than 10% are found to the south of this high potential vorticity region and values exceeding 60% are found to the east. At 400 and 500 mb, the potential vorticity lobes are not as well defined and the maximum values are much smaller (Fig. 3.8b, 3.8c). Relative humidity values of less than 10% and greater than 60% are still present to the south and east of the potential vorticity maximum. By 18 GMT 18 Feb, the potential vorticity maximum at 300 mb has propagated eastward and the same relative humidity pattern that was present six hours earlier is still intact (Fig. 3.9a). The potential vorticity maps at 500 and 400 mb (not shown) are still diffuse while the relative humidities show good continuity in the vertical compared to the previous maps. At 00 GMT 19 Feb (Fig. 3.9b), the potential vorticity lobe has progressed farther to the east and the lobe has decreased in size. The relative humidity regions are in the same positions relative to the potential vorticity lobe. At 06 GMT 19 Feb, the maximum potential vorticity within the lobe has increased slightly and the 60% relative humidity region is protruding toward the center of the lobe (Fig 3.9c). This convergence of high relative humidity into the lobe was also present at 400 and 500 mb (not shown).

The ECMWF vertical motion fields based on the kinematic method are also examined to detect the downward extrusion (subsidence) that should be coincident with high values of potential vorticity. However, the vertical motion fields are extremely noisy and no indication of subsidence is present. It is concluded that vertical motion fields with a 1.875 degree resolution between grid points are not useful in identifying a feature on a scale as small as a tropopause fold.

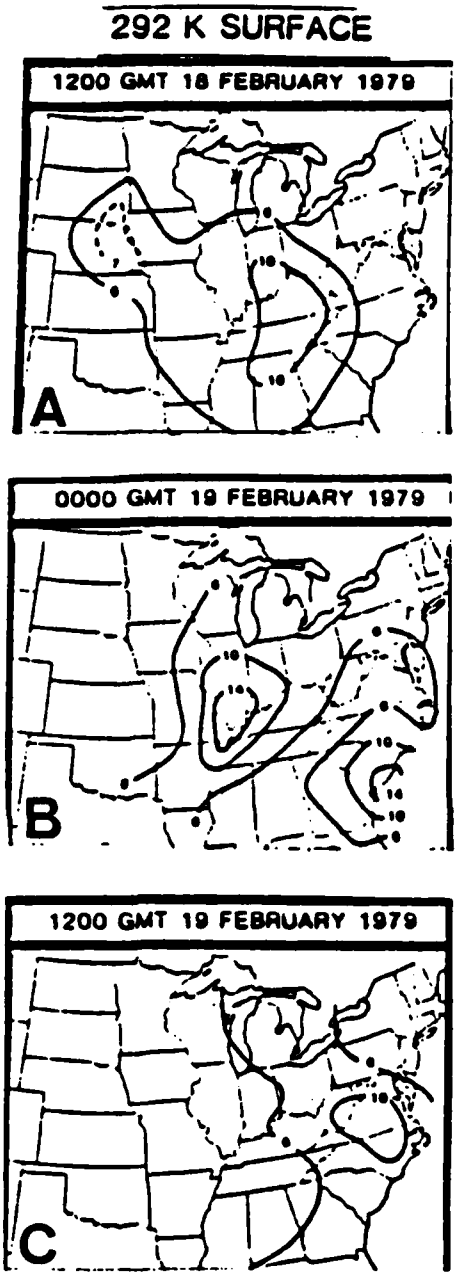

Fig. 3.6 Potential vorticity ($x10^6$ °K/s/mb) analyzed on 292°K surface. See description in text (Uccellini et al. 1985).

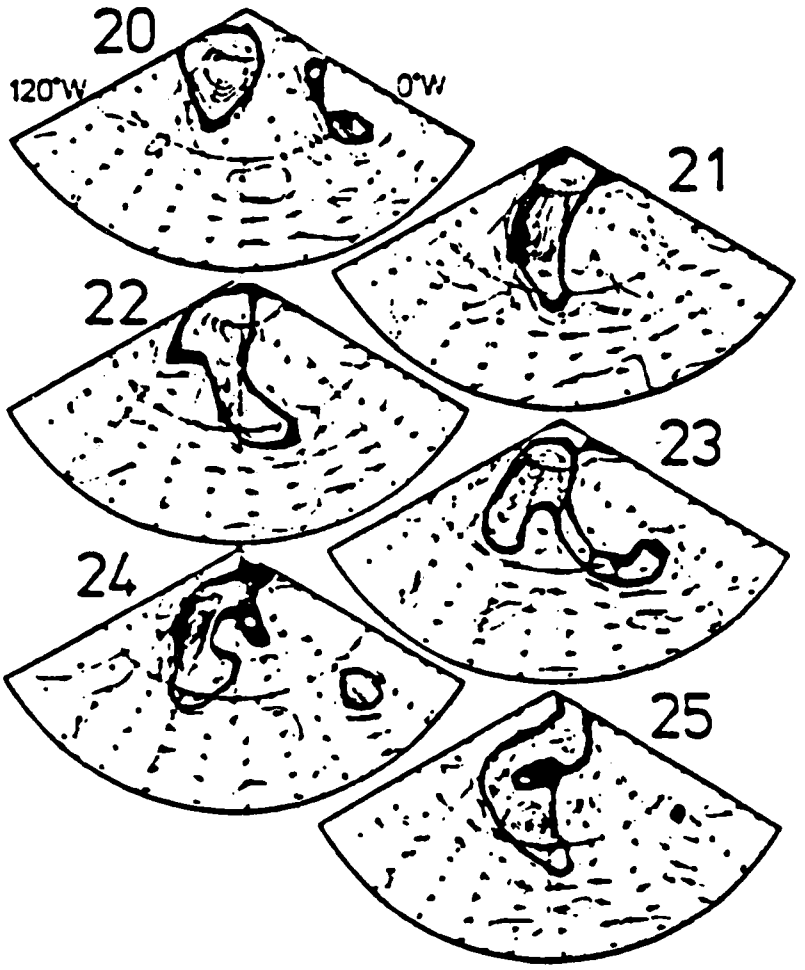

Fig. 3.7 Sectors of the 300°K IPV maps for the period 20-25 Sept 1982. See description in text (Hoskins, 1985).

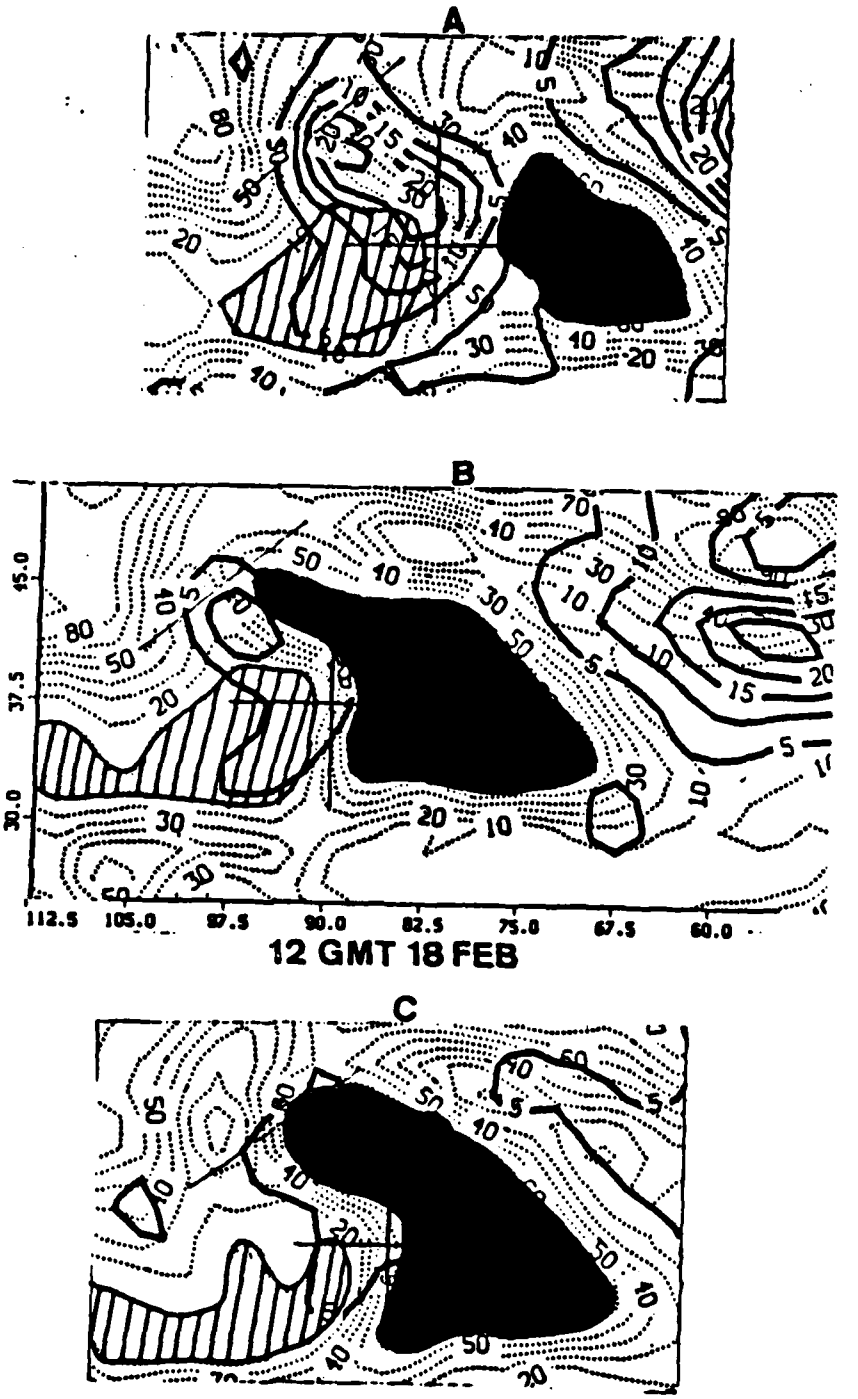

Fig. 3.8 Potential vorticity (solid) ($x10^6$ °K/s/mb) and relative humidity % (dotted) for 300 mb (top), 400 mb (middle), and 500 mb (bottom) at 12 GMT 18 Feb 1979. Solid (dashed) shading depicts relative humidity greater than (less than) 60% (10%).

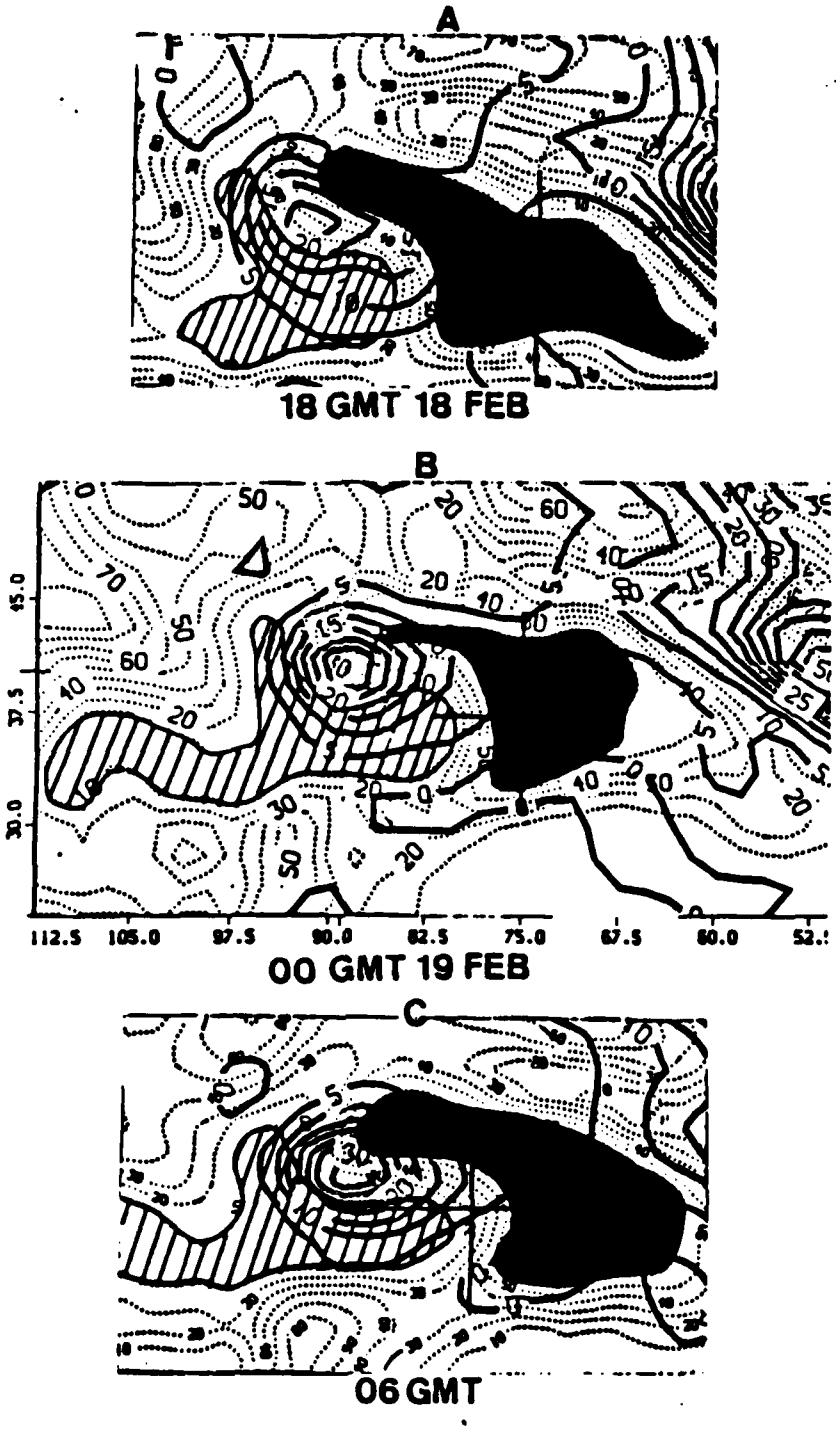

Fig. 3.9 As in Fig. 3.8, except for 300 mb at 18 GMT 18 Feb (top), 00 GMT 19 Feb (middle) and 06 GMT 19 Feb 1979 (bottom).

In summary, an analysis of potential vorticity on pressure surfaces demonstrates that, for the Presidents' Day storm, localized areas of high potential vorticity could be identified and tracked over time. Regions of low and high relative humidity in the ECMWF analyses which are primarily just the first-guess values from the prediction models maintain a consistent location relative to the potential vorticity maximum with time. Thus, relative humidity may serve as another indicator of the region with an intrusion of high potential vorticity associated with a tropopause fold. Since relative humidity data are unavailable for the 23 cyclones of interest, further studies of this humidity pattern as an indicator of high potential vorticity are suggested. Finally, since vertical motion calculations are inherently inaccurate on a small scale, it is not feasible to detect a tropopause fold via the vertical motion field.

The complete vertical structure of a tropopause fold can not be detected from the ECMWF analyses at the mandatory levels. However, the existence of the precursor conditions for cyclogenesis are revealed on the horizontal maps of potential vorticity at 300 mb. Thus, these maps will be examined for the 23 cases of cyclogenesis that were studied by Smith (1986).

IV. RESULTS

A. BACKGROUND

Previous reseachers have studied potential vorticity effects on explosive cyclogenesis on a case-by-case basis (Gyakum, 1983; Hoskins et al., 1985; Uccellini et al., 1985). Uccellini's analysis of the Presidents' Day case emphasizes that a tropopause fold with high potential vorticity had occurred 12 to 24 hours prior to cyclogenesis rather than during the cyclogenetic period as has been noted in previous studies (Bleck, 1973, 1974; Staley, 1960). In the Presidents' Day case an amplifying polar-jet trough system extruded stratospheric air marked by high values of potential vorticity down to the 700 mb level at least 1500 km upstream of the east coast of the U.S. Explosive cyclogenesis occurred when the jet and its associated high potential vorticity moved to a position just upstream of the surface cyclone.

This study examines the 300 mb potential vorticity and jet streaks associated with 23 cyclones in the Alantic and Pacific Oceans that displayed varying degrees of development. By studying numerous cyclones, it is hoped that common characteristics of the potential vorticity and jet streak contributions to explosive cyclogenesis will be sufficiently general to allow development of a forecast aid. The 300 mb potential vorticity and jet streak analyses are available from the ECMWF analyses at six-hour intervals for a minimum of 30 hours. Storm center positions and central pressures (Table 1) were extracted from the NMC final surface analyses by Smith (1986).

In addition to potential vorticity, the 300 mb jet streaks in the vicinity of the cyclones are examined. Pagnotti and Bosart (1984) compared a weak and a strong cyclone along the east coast of the U.S. and found that the stronger cyclone was characterized by significant upper-level forcing associated with a distinct jet trough system. Other studies have shown that jet streaks often play an important role in the development of cyclones (Hovanec and Horn, 1975; Newton, 1956; Reiter, 1969). Uccellini et al., (1985) in his study of the Presidents' Day storm found that the polar front jet (PFJ), the subtropical jet (STJ) and the low-level jet appeared to play important roles in the development of two separate areas of heavy snow. Smith (1986) also found that upper-level divergence is nearly twice as large for the average explosive storm as for the non-explosive storm. Larger sea-level pressure falls are found with

greater divergence aloft for the average explosive storm. Although divergence is not computed in this study, regions of divergence aloft can be inferred from the jet streak analyses.

The evolution of isentropic potential vorticity (referred to as IPV in this chapter so as not to be confused with positive vorticity advection, PVA) and the 300 mb jet streaks associated with five of the 23 storms will be described below. Included in the 23 cases were four storms (P2, P3, A2, and A3) that displayed characteristics similar to the Presidents' Day case in the sense that a distinct pre-existing potential vorticity lobe became superposed with a surface cyclone. The Presidents' Day case will be presented first, and this discussion is followed by two more storms that fit into this category. In the remaining 18 cases, the storm and the IPV maximum to the west appeared to develop concurrently. Two of these cases will be examined in detail. Then, an overall summary of the IPV and jet streak contributions to all 23 cyclones is presented.

B. CASE STUDIES

To provide a background for the following cases, the horizontal maps of IPV (3.1), for the well-analyzed Presidents' Day cyclone will be described. An isolated IPV maximum associated with a polar front jet is approximately 800 n mi to the northwest of a 1016 mb closed low that is located on the anticyclonic side of a 60 m/s jet (Fig. 4.1a). During the next six hours, the IPV maximum closes to within 500 n mi of the cyclone and the sea-level pressure fell to 1012 mb. Although the northerly track of the cyclone still placed it on the anticyclonic side of the jet, the 300 mb winds above the center have increased to 60 m/s (Fig. 4.1b). By 12 GMT 19 Feb (Fig. 4.1c), the IPV maximum has moved just to the northwest of the storm as the sea-level pressure continued to fall to 1004 mb. Bosart (1981) reconstructed the mesoscale features of the storm and determined that actual pressure falls were larger than those depicted on the NMC analyses. The northerly track of the storm along the east coast of the U.S. places it on the cyclonic side of the jet. The storm moves northward around the eastern edge of the IPV lobe and is directly to the east of the maximum as the sea-level pressure drops to 994 mb (Fig. 4.1d). The 60 m/s jet has further decreased in size as the storm is now in the left-front quadrant of the jet streak. The apparent decrease in the jet intensity at 300 mb may be a result of the descending cold dome and the associated jet streak to lower levels. The 300 mb winds above the storm are now only 30 m s due to the storm's movement away from the jet. By 12 GMT 20 Feb (Fig. 4.1e),

the storm is to the east-northeast of the IPV maximum and the pressure drop during the previous 12 hours has been only 4 mb. Some notable observations from this storm are: 1) the lobe of high IPV forms far to the west of the developing cyclone, which distinguishes the development of this storm from other storms that experience concurrent development of the high IPV region and the surface cyclone; 2) the storm movement is counter-clockwise from a position to the southeast of the IPV lobe to the northeast of the lobe over a 36 hour period; 3) the largest pressure falls occur while the storm is to the southeast of the IPV lobe and smaller pressure falls are evident when the storm center is northeast of the lobe; 4) larger pressure falls occur when the storm moves from the anticyclonic to the cyclonic side of the jet; and 5) pressure falls subsequently decrease as the storm moves northward into an area where upper-level winds are lower. Although geopotential height analyses are not referenced in this discussion, a sharply curved developing upper-level short wave trough is a major source of IPV which increases when a jet streak is also present. In this example, storm intensification is greatest when it is to the southeast of the IPV maximum and is consistent with quasi-geostrophic theory which predicts maximum storm development to occur when it is between the trough and the downstream ridge.

An example of a case that is similar to the Presidents' Day storm in which an eastward propagating IPV maximum overtakes an already developed closed low also shows a vagary in the wind field that distorts the IPV maximum. A well-defined maximum at 35° N/ 120° E appears to be located in the left-rear quadrant of the STJ jet (Fig. 4.2a). However, this IPV maximum may be actually a reflection of a smaller jet streak which only becomes evident 12 hours later. This IPV lobe developed in situ and is completely separate from the high IPV reservoir to the north. No surface disturbance is present in the vicinity of the lobe. At 12 GMT 25 Jan (Fig. 4.2b), a 1012 mb closed low develops at the surface as the IPV lobe is 600 n mi to the west. The maximum potential vorticity within the lobe increases and a small 70 m/s jet streak develops so that the cyclone is in the left-front quadrant of the jet streak. In the following 12 hours, the cyclone pressure falls to 1004 mb as the IPV maximum arrives at a position just to the north of the storm (Fig. 4.2c). The apparent decrease in the maximum IPV is due to a poorly represented wind field that distorts the 60 m/s isotach. This example emphasizes the importance of critical evaluation of oceanic data by forecasters since an apparent decrease in potential vorticity in this case is linked to erroneous wind data. The storm is to the south-southeast of the IPV lobe and in the

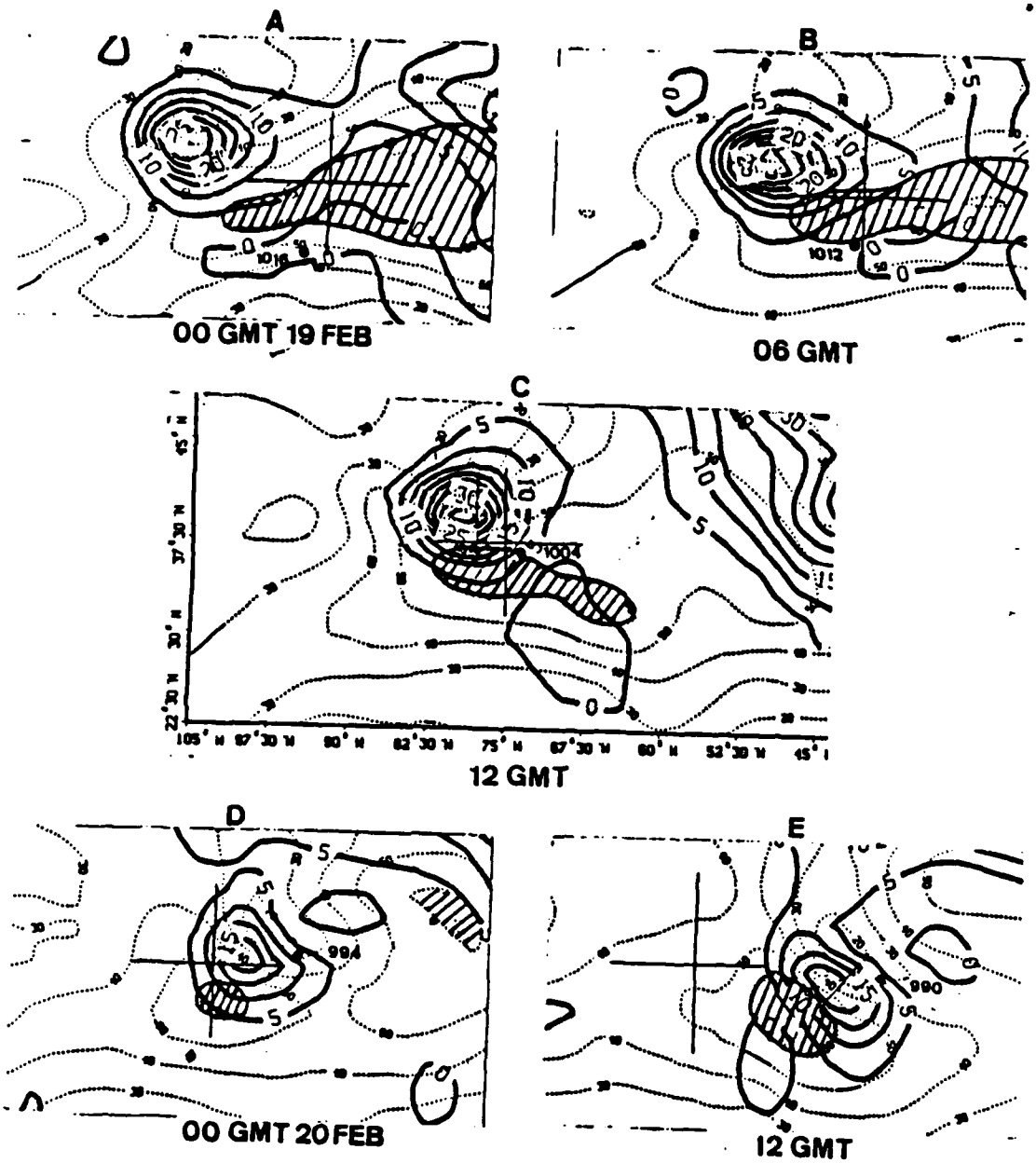

Fig. 4.1 Locations (dots) and central sea-level pressures (mb) from the NMC analyses of an Atlantic cyclone (A-6) relative to 300 mb potential vorticity (solid lines) and winds (dotted). Hatched area represents winds greater than 60 m/s. Positions of panels A,B,D,E are given relative to the cross in panel C at 37.5°N /67.5°W.

left-front quadrant of the jet when the pressure falls to 992 mb during the next 12 hours (Fig. 4.2d). An apparent decrease in the IPV maximum is again due to a poorly represented wind field. By 00 GMT 27 Jan (Fig. 4.2e), the IPV lobe is much better defined than it was during the previous 24 hours as the wind analysis is now more representative. The storm is still in the left-front jet quadrant and has progressed counter-clockwise to the northeast of the IPV maximum. This storm movement may be inferred from the 18 GMT 26 Jan map (not shown) which has the storm to the east-southeast of the IPV maximum. By 06 GMT 27 Jan (not shown), the storm is still to the northeast of the IPV maximum and the pressure has fallen to 980 mb. The deepening rate then decreases substantially as the pressure stabilized at 978 mb for two consecutive 6 hour periods.

In summary of this storm: 1) a lobe of high IPV originates to the west of where a surface low develops and becomes superposed on the storm, and finally stagnates just to the north of the storm; 2) the trajectory of the storm is counter-clockwise relative to the IPV lobe, and maximum pressure falls occur when the storm is to the south-southeast of the PV lobe and lesser pressure falls occur when the storm is to the north-northeast; 3) as the storm tracks northward away from the STJ, the wind speeds aloft decrease, which perhaps contributes to the reduced pressure falls; and 4) a poorly represented wind field over the ocean directly contributes to erroneous IPV fields which could easily be misleading to the forecaster.

A third example in which an eastward propagating IPV maximum appears to have enhanced explosive development of a cyclone may have involved both a STJ and a PFJ. At 00 GMT 5 Feb, a 1016 mb low near 28° N/ 127° E is situated on the anticyclonic side of a STJ (Fig. 4.3a). The IPV to the north of the jet is relatively low, while a PFJ to the north is transporting relatively high IPV southward. The IPV "reservoir" is a term used to decribe the extensive region of stable, high IPV at high latitudes. In most of the 23 cases studied, the IPV field associated with the STJ is fairly distinct since it is normally well to the south of the reservoir. On the other hand, the more northerly position of the PFJ means that it is sometimes difficult to distinguish between jet- and reservoir-associated IPV. By 12 GMT 5 Feb (Fig. 4.3b), the cyclone has tracked to the northeast and is approximately 450 n mi to the east-southeast of the IPV center. The cyclone is proceeding to the cyclonic side of a 60 m/s jet streak as the IPV lobe continues to approach the storm and the pressure falls 12 mb during the next 12 hours (Fig. 4.3c). At this time the storm is in the left-front

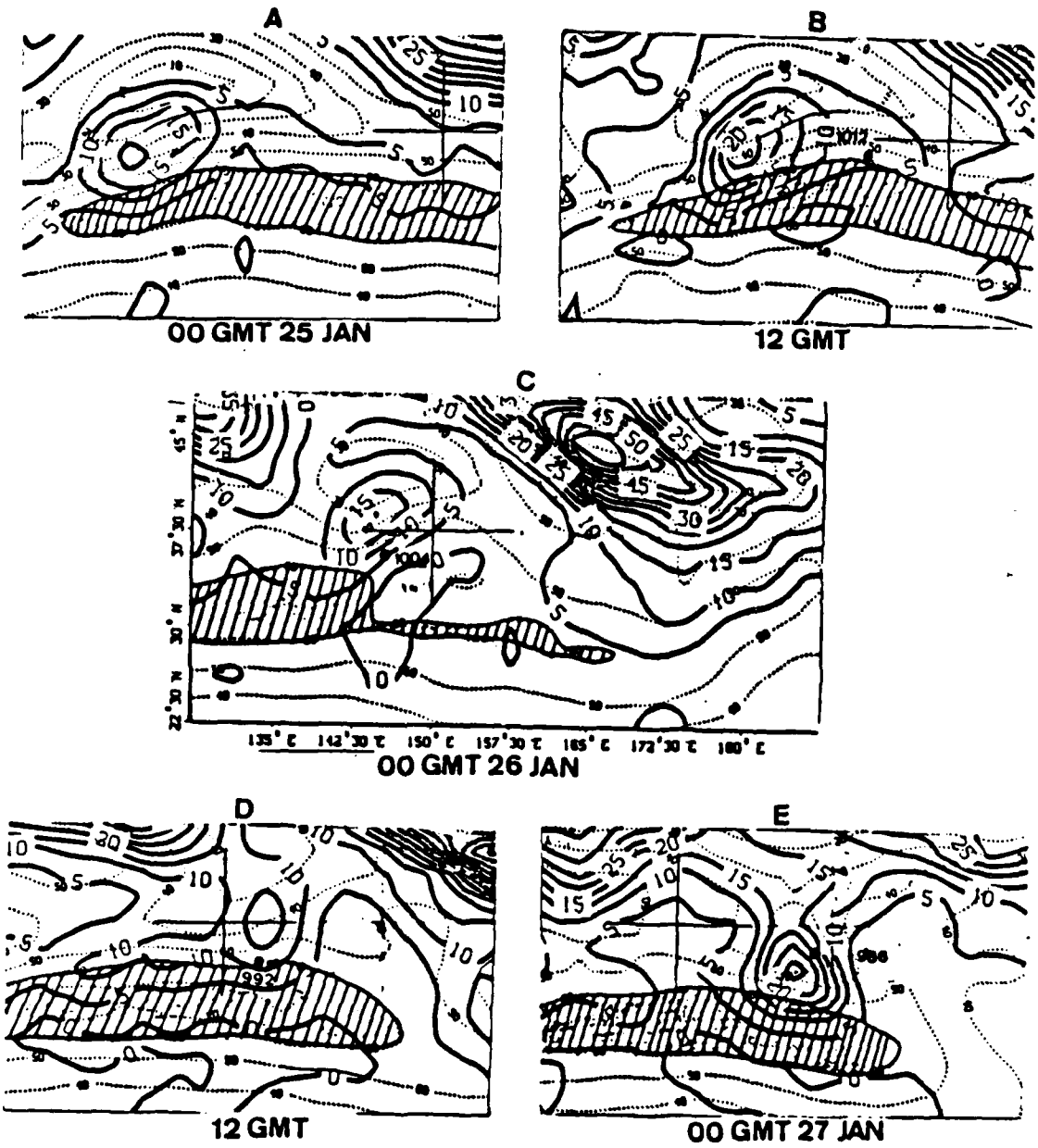

Fig. 4.2 As in Fig. 4.1, except for Pacific cyclone (P-2). Reference position is 37.5°N /150.0°E.

jet quadrant. It is difficult to determine what effect the second IPV maximum associated with the PFJ at 47° N /130° E has on the cyclone's development. The storm is to the east of one IPV maximum and to the southeast of another as the pressure again falls 12 mb in 12 hours (Fig. 4.3d). The two examples above also had large pressure drops when the surface low was located to the east or southeast of an IPV maximum. By 00 GMT 7 Feb (Fig. 4.3e), the pressure falls are diminishing as the storm moves to the northeast of the IPV lobe. However, the further northward movement of the storm is associated with lower winds aloft. This storm development is similar to the previous ones with regard to movement and deepening rates relative to the IPV maximum. This case is somewhat different in that the IPV lobes from both the PFJ and the STJ are present, although it is not clear what effect this had on cyclone development.

In 18 of the 23 cyclones in this sample, development of the cyclone and the IPV to the west are concurrent, in contrast to the Presidents' Day case in which the two appeared to be separate entities. In these 18 cases, a relative IPV maximum is in the vicinity of the surface cyclone as it starts to develop and both propagate eastward at the same speed. One such case that features an extreme deepening rate will now be discussed. A 1013 mb low pressure center is to the east of an IPV maximum that is located between a 70 m/s STJ to the south and a 50 m/s PFJ to the west (Fig. 4.4a). Although the storm is in the left-rear quadrant of the jet, which is a region normally associated with convergence aloft, it is to the east-southeast of the IPV maximum. The pressure falls 13 mb over the next 12 hours (Fig. 4.4b). At this time, the winds above the storm are 80 m/s and the storm maintains a position favorable for development to the southeast of the IPV maximum. The sea-level pressure decreases 10 mb (Fig. 4.4c) as the storm is now in the left-front quadrant of a well-defined jet streak. The tilt of the IPV contours to a more northwest to southeast orientation on the cyclonic side of the PFJ is perhaps indicative of a merging of the two jets. As the winds are almost perpendicular to the IPV contours, strong advection of IPV is present to the east of the maximum. Six hours later, the NMC analyzed central pressure is 960 mb (Fig. 4.4d). Although the precise central pressure may be questioned, extreme deepening of the cyclone obviously did occur. By 00 GMT 11 Feb, the NMC analyzed sea-level pressure is 942 mb (Fig. 4.4e), and this central pressure is maintained for the next six hours (not shown).

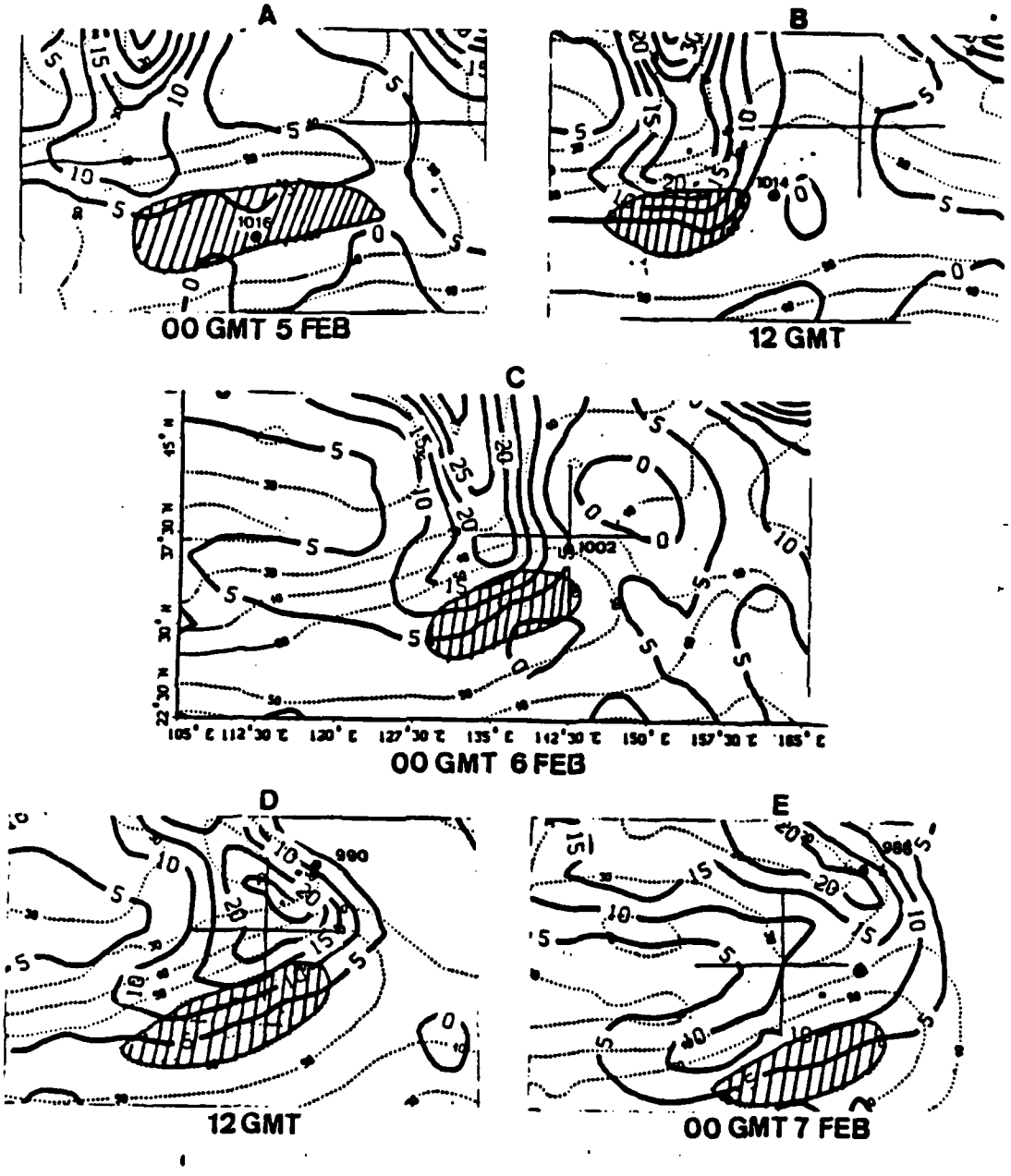

Fig. 4.3 As in Fig. 4.1, except for Pacific cyclone (P-3). Reference position is 37.5°N /142.5°E.

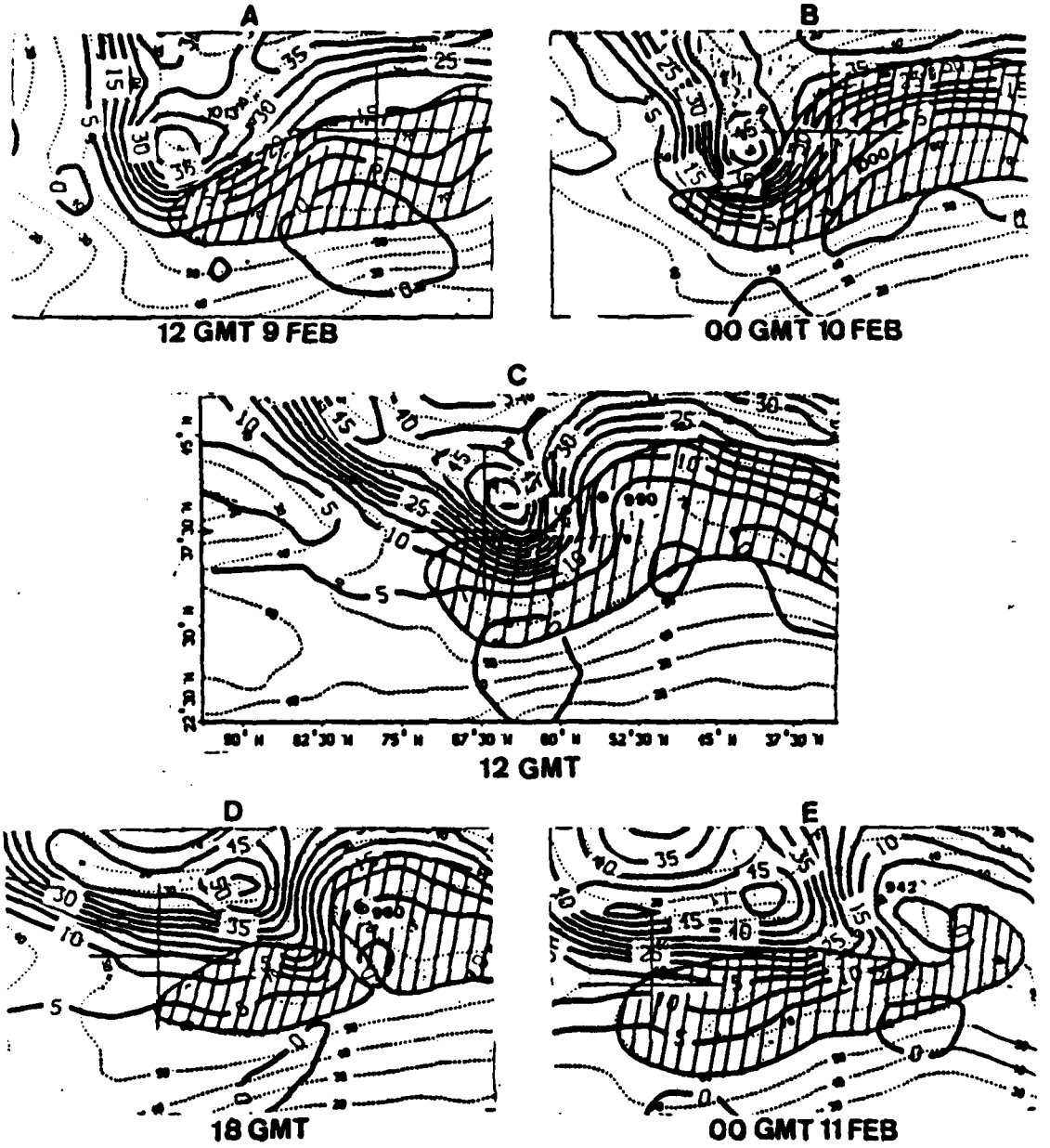

Fig. 4.4 As in Fig. 4.1, except for Atlantic cyclone (A-4). Reference position is 37.5°N /67.5°W.

An analysis of the positive vorticity advection (PVA) for this case shows that the storm starts in a region of positive vorticity advection (Fig. 4.5a). The vorticity advection map (Fig. 4.5b), shows a much more organized PVA center with the storm located near the center. The PVA analysis (Fig. 4.5c) shows the cyclone is still in a region of large positive vorticity advection. Smith (1986) determined that explosively developing storms consistently import greater vorticity aloft than do the non-explosive storms, which results in greater upper-level divergence and larger sea-level pressure falls. The maximum vorticity advection remains to the west of the cyclone (Fig. 4.5d) during the explosive deepening. The diminishing pressure falls correlate with the passage of the maximum in PVA (Fig. 4.5e). Although the areas of positive vorticity advection in this example are well-defined and correlate well with pressure falls, in a majority of the 23 cases the vorticity advection fields are noisy and lack time continuity. However, Smith (1986) indicates that if PVA is area-averaged over 4, 6 and 8 degree radii, a reasonable signature is obtained.

The final case study examines a similar cyclone in which the IPV lobe develops and intensifies without explosive storm development. On 12 GMT 21 Feb, a 1002 mb low is to the north of a relatively small IPV lobe whose maximum value is fairly weak in comparison to the previous cases (Fig. 4.6a). Although the winds above the storm are 25 m/s, a small 50 m/s jet streak is to the south of the storm. Two important factors that are present in the dissipating stage of previously discussed cases are present during the formative stage of this storm. The storm is already to the north of the IPV lobe and the 300 mb winds above the storm are relatively weak. Twelve hours later (Fig. 4.6b), the pressure has dropped only 2 mb. The area of 50 m/s winds to the south and the maximum IPV value have increased slightly, but the storm remains to the north of the lobe and the upper-level winds are still weak. By 12 GMT 22 Feb, the cyclone is near the center of the IPV lobe as the pressure rises to 1003 mb (Fig. 4.6c). In the occluded stage, the storms gradually track toward the center of the lobe where the IPV values are larger. In the next 24 hours, the storm is slightly to the east of the IPV maximum and pressure falls are 4 mb and 1 mb for two consecutive 12 hour periods (Fig. 4.6 d, e). Although the upper-level winds are still weak, the storm has moved to a position where maximum pressure falls have previously been found to occur (east-southeast quadrant). Although this cyclone development is very weak, it follows the pattern in previous storms of small pressure drops when the cyclone position is north of the IPV maximum and relatively weak upper-level winds are present.

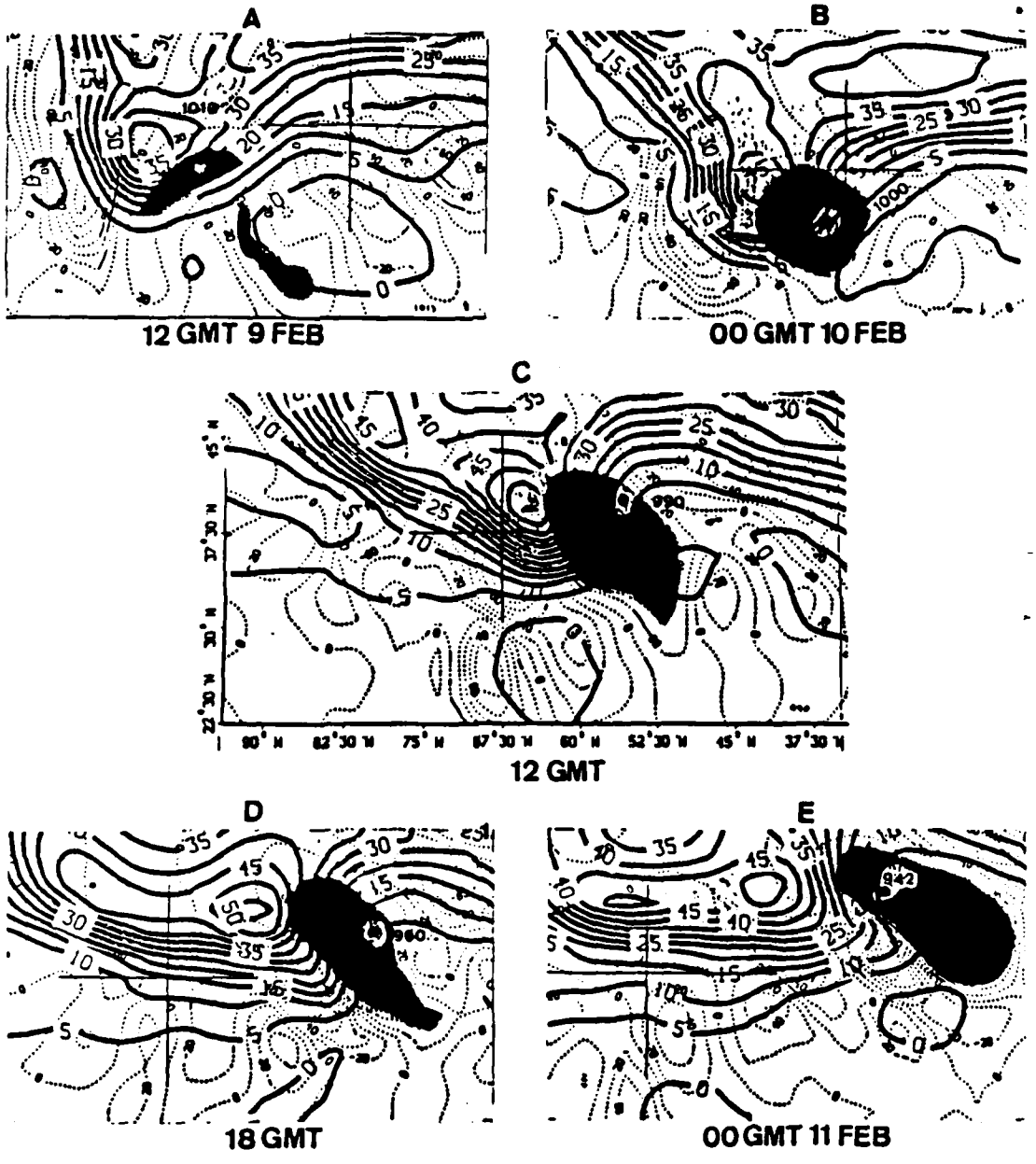

Fig. 4.5 As in Fig. 4.4, except dotted lines represent positive vorticity advection (PVA). Shaded area represents PVA greater than 40 $x10^{-10}$ x s^{-2}.

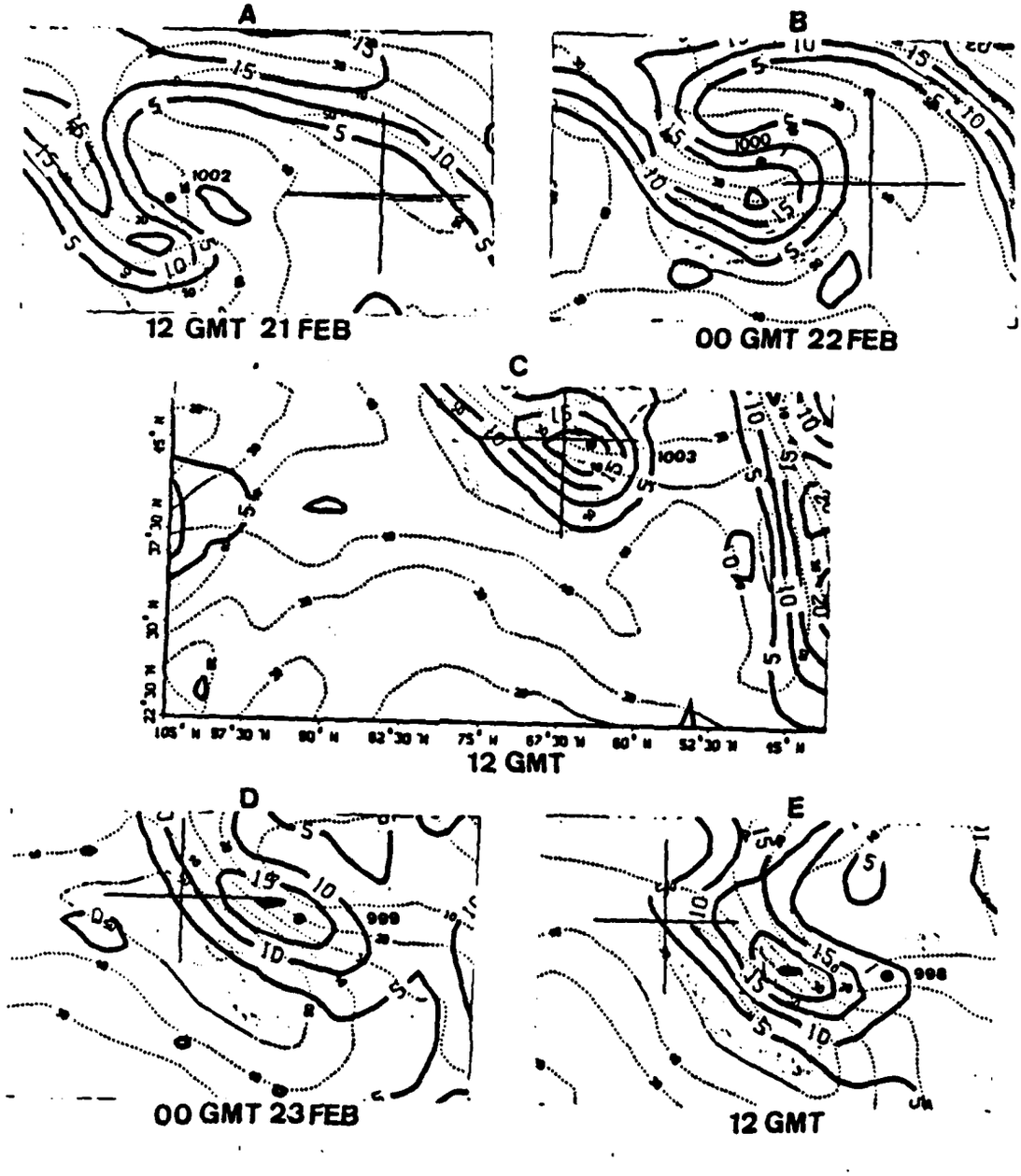

Fig. 4.6 As in Fig. 4.1, except for Atlantic cyclone (NA-2). Reference position is 45.0°N /67.5°W.

Schematic diagrams that illustrate the similarities/ differences in the two types of cyclogenesis cases described above are shown in Figs. 4.7 and 4.8. An example of a case similar to the Presidents' Day case in which the storm and the IPV are separate entities (T+00) is shown in (Fig. 4.7). As the IPV maximum translates eastward with the jet, the relatively weak cyclone proceeds in a generally northerly direction toward the lobe. At T+06, the two features are closer together and the pressure begins to fall as the lobe moves to a position to the east of the center of the STJ. At T+12, the cyclone reaches the point of closest approach to the center of the lobe, the maximum pressure falls occur, and the storm begins a counter-clockwise track relative to the lobe. During the next 18 hours, the storm proceeds to the north of the lobe and the rate of pressure falls decreases. The lobe continues to move to the east relative to the STJ. At T+36, the central pressure has stabilized as the cyclone reaches a position to the north of the lobe and well to the north of the jet streak.

A schematic of the case in which the IPV and the cyclone develop concurrently is shown in Fig. 4.8. In this case, the distance between the IPV maximum and the cyclone is relatively constant. The storm moves counter-clockwise around the IPV maximum and the largest pressure falls occur to the east-southeast of the maximum. Although both the STJ and the PFJ are shown, both need not be present for either of the two cases. In this case, the IPV maximum is still connected to the high IPV reservoir to the north.

C. POTENTIAL VORTICITY AND JET STREAK QUALITATIVE RESULTS

In all of the 23 cyclogenesis cases, relatively high values of IPV are found to the west of the surface cyclone. A subjective, qualtitative analysis of the potential vorticity fields to the west of the 23 cyclones indicated a number of similarities to the above case studies.

The cyclones track counter-clockwise from south to north around the eastern edge of the potential vorticity maximum in 18 of 23 cases. In four cases, the initial storm position is to the north of the IPV maximum and remains there during the development. In each of these four cases the development is rather weak. In the remaining case, the initial position of the storm is well to the south of the IPV maximum and the storm remains stationary.

The storms that track counter-clockwise experience the largest deepening rate when they are to the east or southeast of the IPV maximum. The cyclone intensity

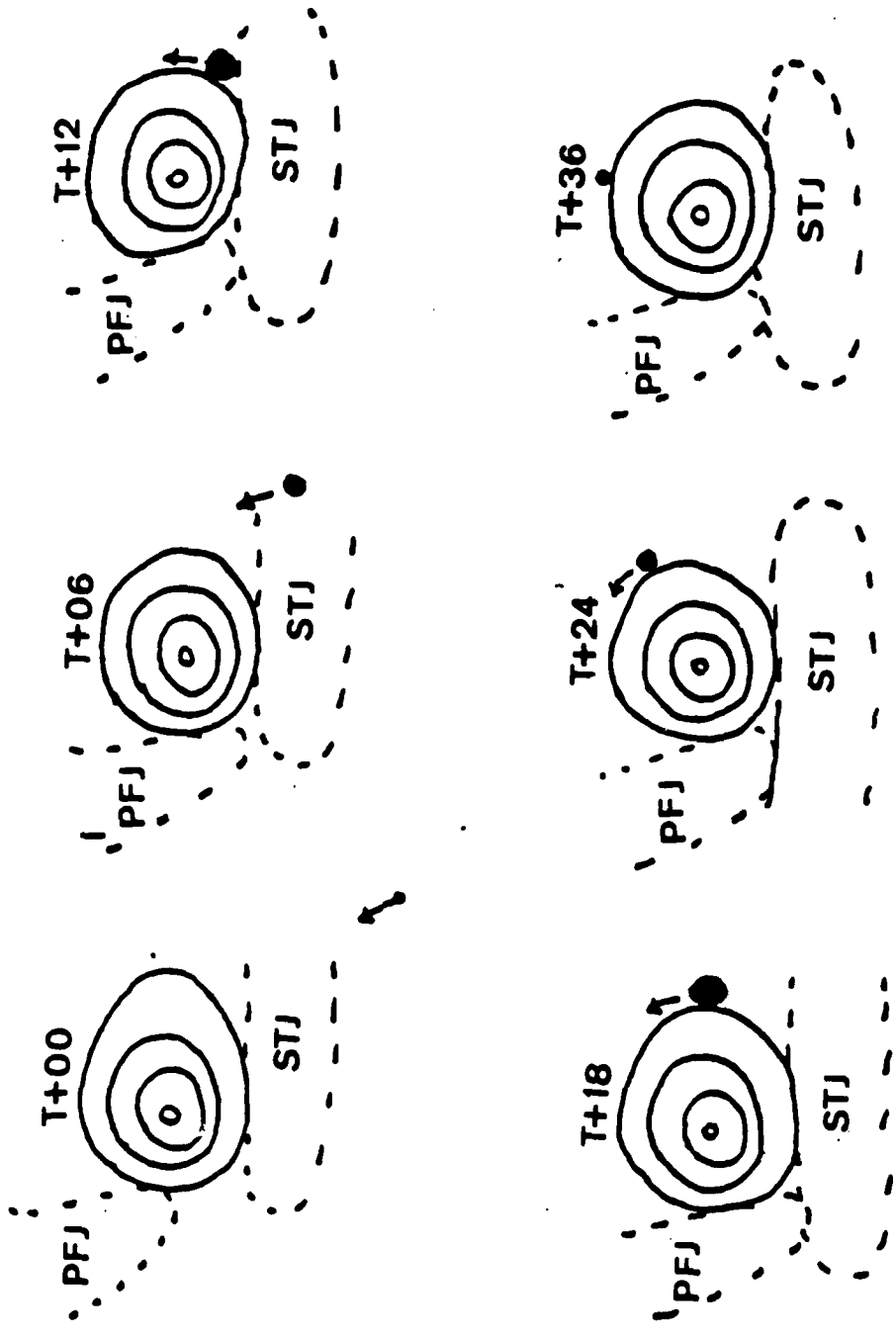

Fig. 4.7 Schematic of potential vorticity lobe (solid) and PFJ and STJ (dashed) relative to the surface cyclone positions in a case similar to the Presidents' Day cyclone. Cyclone intensity is proportional to the dot radius and the direction of motion is indicated by the attached arrow.

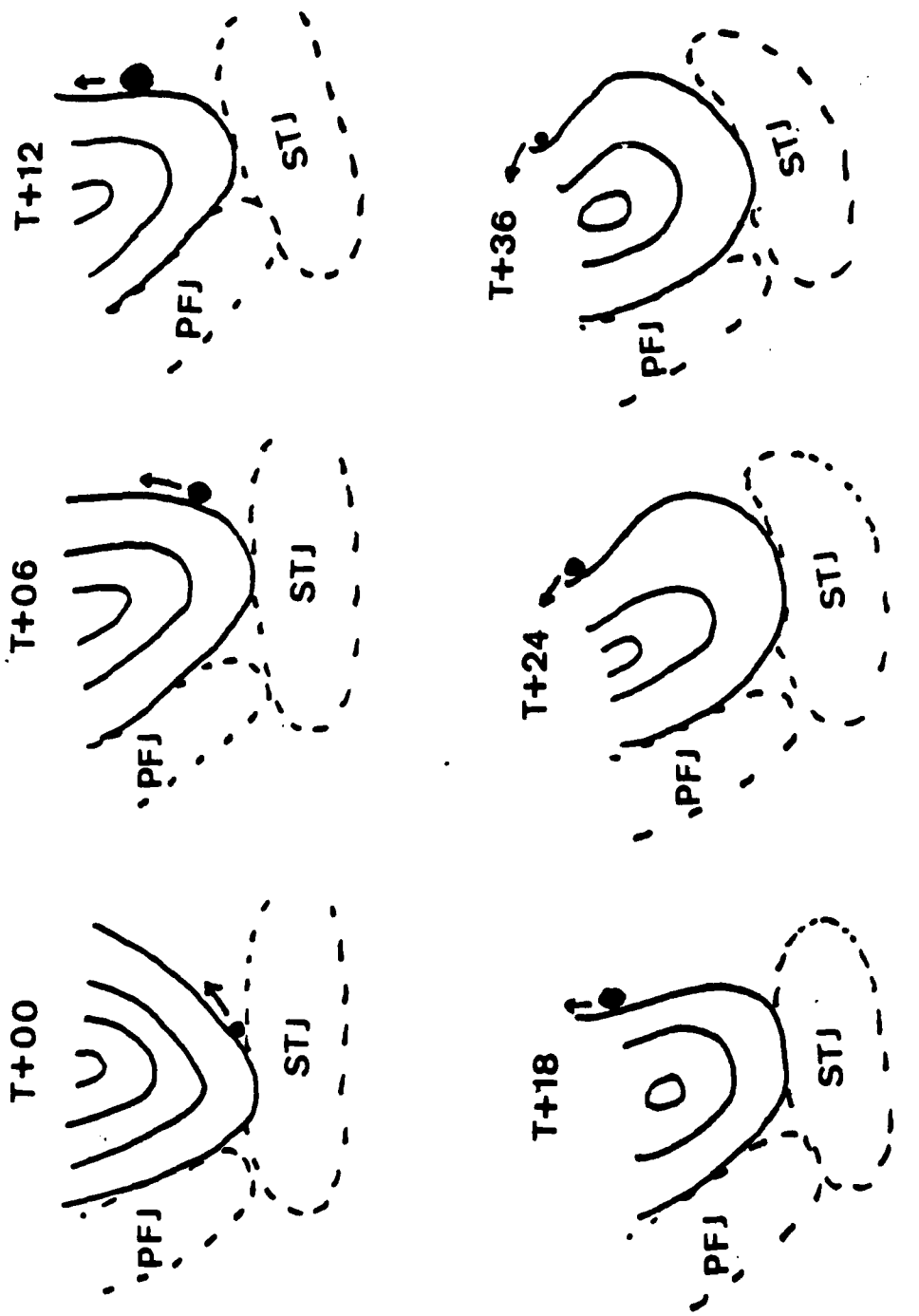

Fig. 4.8 As in Fig. 4.7, except for the case in which the potential vorticity lobe and cyclone develop concurrently.

usually diminishes after reaching a position to the north or northeast of the IPV maximum. Development of the stationary cyclones tends to be rather weak since most of these cyclones are in an unfavorable position to the north of the maximum. When the cyclone is north of the maximum, a 12-hour pressure fall greater than 4 mb occurs in only three instances.

The rate of cyclone deepening does not appear to be a function of the maximum value within the IPV lobe. This observation is consistent with some additional case studies (J.S. Boyle, Naval Postgraduate School). However, the shape and the maximum value in the IPV lobe are highly dependent upon open-ocean analyses, which are often questionable.

Since jet streaks played an important role in the above case studies, the jet streaks associated with the 23 cyclones were analyzed. An attempt is made to determine whether the subtropical jet (STJ), the polar front jet (PFJ), or both are associated with high levels of IPV near a storm region. Factors such as the preferred location relative to the jet for the occurrence of explosive cyclogenesis and the location of maximum IPV values are also explored for the 23 storms below:

In all cases, the highest IPV values are found on the cyclonic shear side of the jet, and normally the maximum IPV is located between the 30 and 50 m/s isotachs. No obvious differences in the maximum IPV between the two types of jets are observed. Although the largest cyclonic shear within a jet is normally located midway along the length of the jet, the position of the maximum IPV is not necessarily at the midpoint. Eleven cases are observed in which the IPV lobe remains in the same position relative to the jet streak. Of these 11 cases, six lobes are found in the left-front jet quadrant, four are found in the middle quadrant, and one is found in the rear quadrant. Of the remaining 12 cases, 10 IPV maxima moved toward the exit region. The presence of high IPV in the left-front jet quadrant coupled with strong upper-level divergence in this quadrant will enhance development of a cyclone below this region.

The IPV maxima that contribute to the 23 cases of cyclogenesis are associated with the PFJ in ten cases, with the STJ in eight cases, and with a combination of both jets in five cases. The STJ is generally at a lower latitude (south of 32° N) and is more consistent in speed (60-70 m/s) and direction (nearly zonal) than the PFJ in these cyclogenesis cases.

The cyclones tend to dissipate as they move northward away from the jet and into an area where the upper-level winds are relatively weak. The correlation between

the strength of the upper-level winds and the pressure fall is relatively high (to be discussed further in Chap. 5).

In 13 cases, the storm remains in the left-front quadrant of the jet. In seven cases, the storm starts in another quadrant and eventually tracks into the left-front quadrant. This includes three cases in which the storm comes from the right-front quadrant and four cases in which the storm comes from the left-rear quadrant. Since 20 of 23 cyclones either remained entirely within the left-front jet quadrant or moved into it, this is indeed a favorable region for cyclogenesis, as was also found in many continental case studies (e.g., Sechrist and Whittaker, 1979) and in a case of maritime explosive cyclogenesis by Calland (1983). In the remaining three cases, a storm develops in each of the other three quadrants. Two of these storms were classified as "non-explosive" by Smith (1986).

In summary, jet streaks appear to be a factor in all 23 storms studied. Both the PFJ and the STJ play nearly equal roles in generating IPV maxima that are present to the west of developing cyclones. The IPV maxima are found within the largest wind gradient region on the cyclonic side of the jet and are generally in the left-front quadrant. In almost all cases, storm development occurs almost entirely in the left-front jet quadrant. In those cases in which the storms cross into this quadrant from the anticyclonic side, large pressure falls subsequently occur. Finally, the rate of deepening decreases as the cyclones move northward away from the jet's influence and into a region of weaker winds aloft.

V. STATISTICAL RESULTS

To provide more quantitative measures, a statistical analysis of 6-h and 12-h pressure falls using NMC data is performed. A sample of 78 surface pressure changes from the Pacific storms and 71 from the Atlantic storms forms the predictands. The predictors are the current values of:

1) the latitude of the cyclone
2) positive vorticity advection (PVA) at 300 mb directly above the cyclone
3) 300 mb wind speed
4) 300 mb potential vorticity
5) distance (n mi) from the cyclone to the nearest potential vorticity contour of $30° K \times s^{-2} \times mb^{-1}$, which is the typical maximum in potential vorticity; and
6) potential vorticity quadrant, which is the bearing of the cyclone relative to the upstream potential vorticity maximum within 22.5° sectors numbered clockwise from north (0), through east-southeast (5), and then decreasing to south (2). The largest value is assigned to the east-southeast quadrant since the greatest pressure falls are normally observed in this quadrant.

A standard stepwise regression routine is used to determine which variables are significantly correlated with the observed sea-level pressure decreases (Table 2). The independent variables are entered (forward stepped) one at a time based on the maximum partial correlation coefficient. The correlations are generally higher for the 12-h than for the 6-h pressure falls. Since the central pressures are only known to a few mb, the shorter interval contains a smaller signal-to-noise component.

The correlations for most of the variables are similar with the Atlantic sample having slightly larger values than the Pacific sample. The highest total explained variance (0.38) is found in the Atlantic 12-h category. This relatively low value is probably due to noisy predictands and perhaps to the absence of low-level predictands such as baroclinicity, thermal advection, or conditional instability measures. A negative correlation of central pressure falls with latitude indicates that cyclones tended to have larger deepening rates at southern latitudes, perhaps due to a larger convective contribution over warmer water. Smith (1986) also noted this tendency.

TABLE 2. CORRELATIONS OF VARIABLES WITH 6- AND 12-H PRESSURE FALLS

Correlations of variables with 6- and 12-H pressure falls in the Pacific and Atlantic Oceans. The variables entered are the variables found to be the most significant in determining pressure falls in each category. The explained variance is the percentage of the total variance explained by each of the variables entered.

	6 HOUR		12 HOUR	
VARIABLES	PACIFIC	ATLANTIC	PACIFIC	ATLANTIC
LATITUDE (DEG)	-0.17	-0.25	-0.30	-0.43
PVA (1/SEC X SEC)	0.25	0.29	0.20	0.29
WIND SPEED (M/S)	0.31	0.37	0.45	0.48
POTENTIAL VORT. (DEG. K/SEC/MB)	-0.22	-0.21	-0.31	-0.36
POTENTIAL VORT. QUADRANT (PQUAD)	0.34	0.40	0.53	0.62
DISTANCE (N MI)	-0.01	-0.15	0.10	-0.11
		REGRESSION EQUATIONS		
VARIABLES ENTERED	PQUAD,PVA	PQUAD	PQUAD,LAT	PQUAD
EXPLAINED VARIANCE	0.11,0.05	0.16	0.28,0.05	0.38
TOTAL EXPLAINED VARIANCE	0.16	0.16	0.33	0.38

The negative correlation of central pressure tendency with potential vorticity indicates that the higher values of potential vorticity tend to be more coincident with the cyclone as it becomes occluded. The distance between the cyclone and the 30 unit potential vorticity value is not significantly correlated with the pressure drops. This means that a forecast of more rapid deepening of a storm based solely on the distance to the potential vorticity maximum is not justified. Rather, the relative orientation of the surface cyclone and the potential vorticity maximum is more important.

Based on the stepwise regression, the potential vorticity quadrant is the most significant single variable in the Atlantic and the Pacific samples. Positive vorticity advection (PVA) is also significant in the Pacific sample of 6-h pressure falls and latitude is also significant in the Pacific 12-h category. Other variables do not enter as they do not provide independent information.

To determine if current values of the previously defined variables can be used to accurately predict changes in the sea-level pressure over 12 hours, a regression equation is derived based on a least-squares best fit of the variables. One hundred 12-h surface pressure changes are randomly selected from the total sample size of 149 from the Atlantic and Pacific. From this dependent sample, the predicted pressure change (PRED) is expressed as a function of the two variables PVORT and PQUAD which have the greatest influence on the pressure change.

$$\text{PRED} = 1.634 - 0.129\ \text{PVORT} + 2.257\ \text{PQUAD}.$$

This equation is applied to the 49 pressure changes in the independent sample. The correlation coefficient between the predicted and the actual pressure changes in the independent sample is 0.62, or an explained variance of 0.38. The mean value of the actual pressure changes (6.3 mb) is slightly less than the mean of the predicted changes (7.1 mb) and the standard deviations are 5.9 mb and 3.6 mb respectively. Although the explained variance is relatively low, the fact that the standard error of estimation (4.7 mb) is less than the standard deviation of the actual pressure change (5.9 mb) is significant. These regression equation attempts indicate the difficulty in forecasting actual numerical pressure falls and provide motivation for doing discriminate analysis within the categories.

A discriminate analysis is also performed on the same variables to determine whether the storm development over a 12-h period could be forecast in one of three categories of development. Based on the histogram of the central pressure decreases which included approximately 25 in each category, the following three categories are derived:

1) Low - pressure falls of less than 4 mb in 12-h for the Atlantic and Pacific;

2) Moderate (Mod) - pressure falls between 4-10 mb in 12-h for the Atlantic, and between 4-8 mb in 12-h for the Pacific;

3) Explosive (Exp) - pressure falls greater than 10 mb in 12-h for the Atlantic, and greater than 8 mb in 12-h for the Pacific.

Mean values of the variables for low, moderate, and explosive developments in terms of 12-h pressure falls are given in Table 3. The explosive cases tend to occur in the lower latitudes, although the large standard deviations in these categories indicates that the differences may not be significant. Smith (1986) found the same relationship between latitude and explosive cyclogenesis.

Positive vorticity advection (PVA) is also large for the explosive cases. This result is also consistent with Smith (1986).

Larger 300 mb wind speeds are found in the explosive cases. This result is shown by the relatively high correlation of wind speed and pressure drop (PDROP) for the 12-h samples (Table 2).

Cases of explosive development tend to have low potential vorticity values, as expected from the negative correlation between potential vorticity and pressure falls in Table 2. As the pressure falls stabilize during the occluded stage, the cyclone center tends to be located beneath a lobe of maximum potential vorticity.

Storms develop most rapidly to the east-southeast of a lobe of maximum potential vorticity. This is evident from the mean potential vorticity quadrant values of 4.3 for both oceans in the 12-h explosive category (Table 3). Storms with low deepening rates are generally found to the north or northeast of the potential vorticity maximum. This result is also consistent with the case studies in the previous chapter.

The lack of consistency in the distances of the storms from the 30 unit potential vorticity contour (Table 3) is also evident in the low correlation values from Table 2. The standard deviations of the distances are almost as large as the mean values.

A contingency table of the number of storms that are correctly forecast in each category using the discriminate analysis is shown in Table 4. In both 12-h categories, the potential vorticity quadrant (PQUAD) is the only predictor selected in the discriminate analysis. Perfect forecasts lie along the diagonal from the upper left to the lower right corner. A purely random selection would place about 11% in each of the nine possible categories, or about 33% correct. The results here are clearly better than random choice. Using these results, a forecaster can input a value for PQUAD into

each of three probability equations for Low, Mod and Exp developing cyclones and select the category with the highest value as the most likely storm development during the next 12 hours. The predicted categories of development in Atlantic and Pacific storms relative to the IPV maxima are summarized in Fig. 5.1.

The explosively developing cyclones have the highest forecast accuracy in both 12-h categories with the Atlantic category having the highest percentage (90.5%). Both the explosive and low developers are more consistently discriminated in comparison to the moderate developers. The number of 12-h forecasts that are in error by more than one category is fairly low. For example, only 9 of the 78 Pacific cases and only 6 of the 71 Atlantic cases are incorrectly classified by two categories. It is particularly encouraging that only one of the 26 (21) Pacific (Atlantic) 12-h explosive developers is incorrectly classified into the low category.

TABLE 3. MEAN VALUES AND STANDARD DEVIATIONS OF VARIABLES

Mean values of the variables for low, moderate (Mod) and explosive (Exp) categories of 12-H pressure falls for Atlantic (ATL) and Pacific (Pac) samples. Standard deviations are in parentheses below the mean. Units are same as Table 2.

	12 HOUR PRESSURE FALL		
	LOW PAC/ATL	MOD PAC/ATL	EXP PAC/ATL
LATITUDE	42.3/45.0	39.9/39.0	38.3/37.3
	(5.0/6.9)	(5.7/4.7)	(3.4/5.6)
PVA	27.0/17.4	26.6/31.3	47.9/37.8
	(19.3/32.6)	(26.9/40.8)	(37.1/30.0)
WIND SPEED	33.0/31.1	40.5/44.9	48.5/56.4
	(12.8/19.0)	(12.2/18.0)	(10.5/14.7)
POTENTIAL VORTICITY	14.7/20.1	12.1/12.2	8.5/10.8
	(9.1/11.6)	(7.4/9.3)	(7.7/9.6)
POTENTIAL VORT. QUADRANT	2.7/1.9	3.1/3.2	4.3/4.3
	(1.2/1.9)	(1.1/1.1)	(0.8/0.8)
DISTANCE	271/444	425/324	400/284
	(300/486)	(286/290)	(269/184)

TABLE 4. FORECAST VS. OBSERVED CENTRAL SURFACE PRESSURES

Forecast vs. observed central surface pressures in three categories as determined by discriminate analysis (low, moderate-Mod, and explosive-Exp) of cyclone development.

PACIFIC 12 HOUR

		FORECAST			
		LOW	MOD	EXP	% CORRECT
OBSERVED	LOW	10	5	8	43.5
	MOD	9	7	13	24.1
	EXP	1	2	23	88.5
			OVERALL PERCENT CORRECT		51.3

ATLANTIC 12 HOUR

		FORECAST			
		LOW	MOD	EXP	% CORRECT
OBSERVED	LOW	13	1	5	68.4
	MOD	7	11	13	35.5
	EXP	1	1	19	90.5
			OVERALL PERCENT CORRECT		60.6

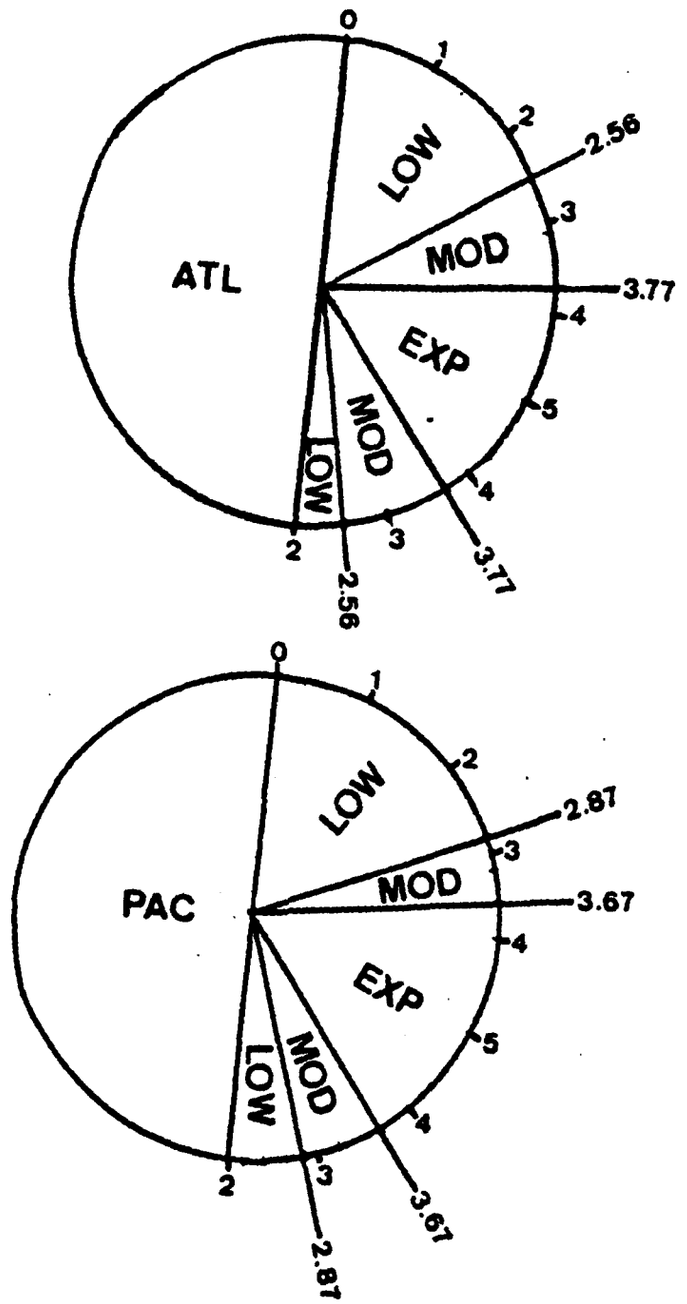

Fig. 5.1 Expected development rates (low, moderate, explosive) of Atlantic (ATL) and Pacific (PAC) cyclones based on the relative bearing of the sea-level pressure center from the center of a 300 mb IPV maximum. The numbers along the sector lines indicate the PQUAD values in the discriminate analysis description in the text.

VI. CONCLUSIONS

To gain insight into jet streak properties that contribute to explosive maritime cyclogenesis, the 300 mb winds and potential vorticity from 23 storms in the Atlantic and Pacific are compared. The wind fields are from ECMWF Level III-b analyses of FGGE data during 17 January 1979 to 23 February 1979. Jet streak features associated with storm development are analyzed every 6-h for a minimum of 30-h prior to and during maximum intensification of the storm.

The objective is to determine whether the explosive deepening of the storms occurred when a region of high potential vorticity that was propagating eastward became superposed over the surface center. Four of the 23 cyclones (the Presidents' Day case being the fifth), develop in a manner similar to the Presidents' Day storm , in which a pre-existing, distinct lobe of high potential vorticity associated with an eastward propagating jet becomes superposed over a surface cyclone prior to explosive development. In the remaining cases, the cyclone and the potential vorticity lobe develop concurrently and track eastward while maintaining the same separation. Storm intensification relative to the potential vorticity maximum progresses in a consistent manner with maximum deepening occurring when the storm is to the east-southeast of the maximum. Pressure falls gradually diminish as the storm progresses counter-clockwise along the eastern edge of the potential vorticity lobe to a position to the north of the maximum. Since relatively high values of potential vorticity are present to the west or northwest of all 23 cyclones in these ECMWF analyses, perhaps this systematic relationship can be used to forecast potential explosive cyclogenesis cases. That is, these precursor conditions might be present in the predicted wind and stability fields of the numerical weather prediction model, even if the model physics or numerics do not allow accurate forecasts of explosive cyclogenesis.

The presence of a jet maxima over the storm is a major factor in storm development with larger pressure falls being related to higher wind speeds. The left-front jet quadrant appears to be important in cyclogenesis since 20 of 23 storms were located within this quadrant at some time during development. Knowledge of the position of a storm relative to the jet streak maximum, the strength of the upper-level winds, and the location relative to the potential vorticity maximum thus might be combined into a useful forecast aid.

The correlations between central pressure falls and the predictors studied are very similar between the two oceans. The correlations are greater for the 12-h than for the 6-h pressure falls. The variable with the highest correlation is the potential vorticity quadrant. The relatively low explained variances from the regression analysis imply that attempting to forecast the actual values of pressure falls based on upper-air variables is very difficult. Consequently, an attempt is made to simply classify the pressure falls as low, moderate and explosive deepeners. It is especially encouraging that the explosively developing storms are classified correctly in about 90% of the cases with very few misclassifications as storms with low deepening rates. The false alarm rates (low developers that were forecast to be explosive) are 10% and 7% for the Pacific and Atlantic respectively.

In future research, the sample size of maritime cyclones should be increased to provide greater statistical significance. A major drawback to oceanic analyses is the lack of significant level rawinsonde data which could define the amplitude and downward extension of the potential vorticity features. Rather than using only upper-level predictors, factors such as low-level moisture and thermal advection should also be included to provide a more complete analysis. Suggestions for follow-on study include using relative humidity fields to aid in the location of tropopause folds and determination of potential vorticity advection effects on explosive cyclogenesis.

This "perfect-prog" study based on ECMWF analyses suggests the feasibility of detecting the precursor conditions for explosive maritime cyclogenesis from operational data. However, the implementation of this procedure must be with actual forecast fields rather than analyses. If it could be shown that the procedure also works well with these forecast fields, the forecaster would have improved guidance for recognizing the explosive deepening stage of maritime cyclones.

LIST OF REFERENCES

Bleck, R., 1973: Numerical forecasting experiments based on the conservation of potential vorticity on isentropic surfaces. *J. Appl. Meteor.*, **12,** 737-757.

———, 1974: Short range prediction in isentropic coordinates with filtered and unfiltered numerical models. *Mon. Wea. Rev.*, **102,** 813-829.

Bosart, L. F., 1981: The Presidents' Day snowstorm of 18-19 February 1979: A subsynoptic scale event. *Mon. Wea. Rev.*, **109,** 1542-1566.

———, and S. C. Lin, 1984: A diagnostic analysis of the Presidents' Day storm of February 1979. *Mon. Wea. Rev.*, **112,** 2148-2177.

Calland, W. E., June 1983: Quasi-Langrangian diagnostics applied to an extratropical explosive cyclogenesis in the North Pacific. M.S. Thesis, Naval Postgraduate School, 154 pp.

Danielsen, E. F., 1968: Stratospheric-tropospheric exchange based on radioactivity, ozone and potential vorticity. *J. Atmos. Sci.*, **25,** 502-518.

Gyakum, J. R., 1983: On the evolution of the QE-II Storm. II: Dynamic and thermodynamic structure. *Mon. Wea. Rev.*, **111,** 1156-1173.

Halem, M., E. Kalnay, W. E. Baker, and R. Atlas, 1982: An assessment of the FGGE satellite observing system during SOP-I. *Bull. Amer. Meteor. Soc.*, **63,** 407-427.

Hoskins, B. J., M. E. McIntyre, and A. W. Robertson, 1985: On the use and significance of isentropic potential vorticity maps. *Quart. J. Roy. Meteor. Soc.*, **111,** 877-946.

Hovanec, R. D. and L. H. Horn, 1975: Static stability and the 300 mb isotach field in the Colorado cyclogenetic area. *Mon. Wea. Rev.*, **103,** 628-638.

Newton, C. W., 1956: Mechanism of circulation change during a lee cyclogenesis. *J. Meteor.*, **13,** 528-539.

Pagnotti, V., and L. F. Bosart, 1984: Comparative diagnostic case study of east coast secondary cyclogenesis under weak versus strong synoptic-scale forcing. *Mon. Wea. Rev.*, **112,** 5-30.

Reed, R. J., 1955: A study of a characteristic type of upper level frontogenesis. *J. Meteor.*, **12,** 226-237.

Reiter, E. R. , 1969: Tropopause circulation and jet streams. *World Survey of Climatology*, **vol.4,** *Climate of the Free Atmosphere* D. F. Rex, Ed., Elsevier, 85-193.

Sanders, F., and J. R. Gyakum, 1980: Synoptic-dynamic climatology of the 'Bomb". *Mon. Wea. Rev.*, **108,** 1589-1606.

Sechrist, F. S., and T. M. Whittaker, 1979: Evidence of jet streak vertical circulations. *Mon. Wea. Rev.*, **107**, 1014-1021.

Shapiro, M. A., 1970: On the applicability of the geostrophic approximation to upper level frontal scale motions. *J. Atmos. Sci.*, **27**, 408-420.

———, 1978: Further evidence of the mesoscale and turbulent structure of upper-level jet stream frontal zone systems. *Mon. Wea. Rev.*, **106**, 1100-1111.

———, 1980: Turbulent mixing within tropopause folds as a mechanism for the exchange of chemical constituents between the stratosphere and troposphere. *J. Atmos. Sci.*, **37**, 994-1004.

Smith, D. H., March 1986: A diagnostic investigation of explosive maritime cyclogenesis during FGGE. M. S. Thesis, Naval Postgraduate School, 54 pp.

Staley, D. O., 1960: Evaluation of potential vorticity changes near the tropopause and the related vertical motions, vertical advection of vorticity, and transfer of radioactive debris from stratosphere to troposphere. *J. Meteor.*, **17**, 591-620.

Uccellini, L. W., P. J. Kocin, R. A. Peterson, C. H. Wash, and K. F. Brill, 1984: The Presidents' Day cyclone of 18-19 February 1979: Synoptic overview and analysis of the subtropical jet streak influencing the pre-cyclogenetic period. *Mon. Wea. Rev.*, **112**, 31-55.

———, D. Keyser, K. F. Brill, and C. H. Wash, 1985: The Presidents' Day cyclone of 18-19 February 1979: Amplification and associated tropopause folding on rapid cyclogenesis. *Mon. Wea. Rev.*, **113**, 962-988.

INITIAL DISTRIBUTION LIST

		No. Copies
1.	Defense Technical Information Center Cameron Station Alexandria, VA 22304-6145	2
2.	Library, Code 0142 Naval Postgraduate School Monterey, CA 93943-5002	2
3.	Chairman (Code 63Rd) Department of Meteorology Naval Postgraduate School Monterey, CA 93943	1
4.	Chairman (Code 68Mr) Department of Oceanography Naval Postgraduate School Monterey, CA 93943	1
5.	Professor R. L. Elsberry (Code 63Es) Department of Meteorology Naval Postgraduate School Monterey, CA 93943	8
6.	Professor C. H. Wash (Code 63Wx) Department of Meteorology Naval Postgraduate School Monterey, CA 93943	1
7.	Professor J. S. Boyle (Code 63By) Department of Meteorology Naval Postgraduate School Monterey, CA 93943	1
8.	LT Peter J. Kirchoffer 135 S. Porter Ave. Waukesha, WI 53186	2
9.	Director Naval Oceanography Division Naval Observatory 34th and Massachusetts Avenue NW Washington, DC 20390	1
10.	Commander Naval Oceanography Command NSTL Station Bay St. Louis, MS 39522	1
11.	Commanding Officer Naval Oceanographic Office NSTL Station Bay St. Louis, MS 39522	1
12.	Commanding Officer Fleet Numerical Oceanography Center Monterey, CA 93943	1

13. Commanding Officer
Naval Ocean Research and Development Activity
NSTL Station
Bay St. Louis, MS 39522 — 1

14. Commanding Officer
Naval Environmental Prediction Research Facility
Monterey, CA 93943 — 1

15. Chairman, Oceanography Department
U.S. Naval Academy
Annapolis, MD 21402 — 1

16. Chief of Naval Research
800 N. Quincy Street
Arlington, VA 22217 — 1

17. Commanding Officer
Naval Eastern Oceanography Center
Naval Air Station
Norfolk, VA 23511 — 1

18. Commanding Officer
Naval Western Oceanography Center
Box 113
Pearl Harbor, HI 96860 — 1

19. Commanding Officer
Naval Oceanography Command Center, Rota
Box 31
FPO San Francisco, CA 09540 — 1

20. Commanding Officer
Naval Oceanography Command Center, Guam
Box 12
FPO San Francisco, CA 96630 — 1

END

2-87

DTIC